VUV and X-ray Free-Electron Lasers

Hard and Soft X-ray Self-Seeding, RAFEL, XFELO, HGHG and EEHG

Dinh Nguyen,[1] Christopher Mayes,[1] Nicole Neveu[2], Colwyn Gulliford[3]
[1] xLight Inc.
[2] SLAC National Accelerator Laboratory
[3] Xelera

Thursday Schedule

• Hard & Soft X-ray Self-Seeding	09:00 – 10:00
• Break	10:00 – 10:10
• Regenerative Amplifier FEL, Oscillator FEL	10:10 – 11:10
• Break	11:10 – 11:20
• Harmonic Generation, HGHG, & EEHG	11:20 – 12:00
• Lunch Break	12:00 – 13:30
• Lab Project	13:30 – 17:00

Hard X-ray Self-Seeding

SASE Is Inherently Chaotic and Noisy

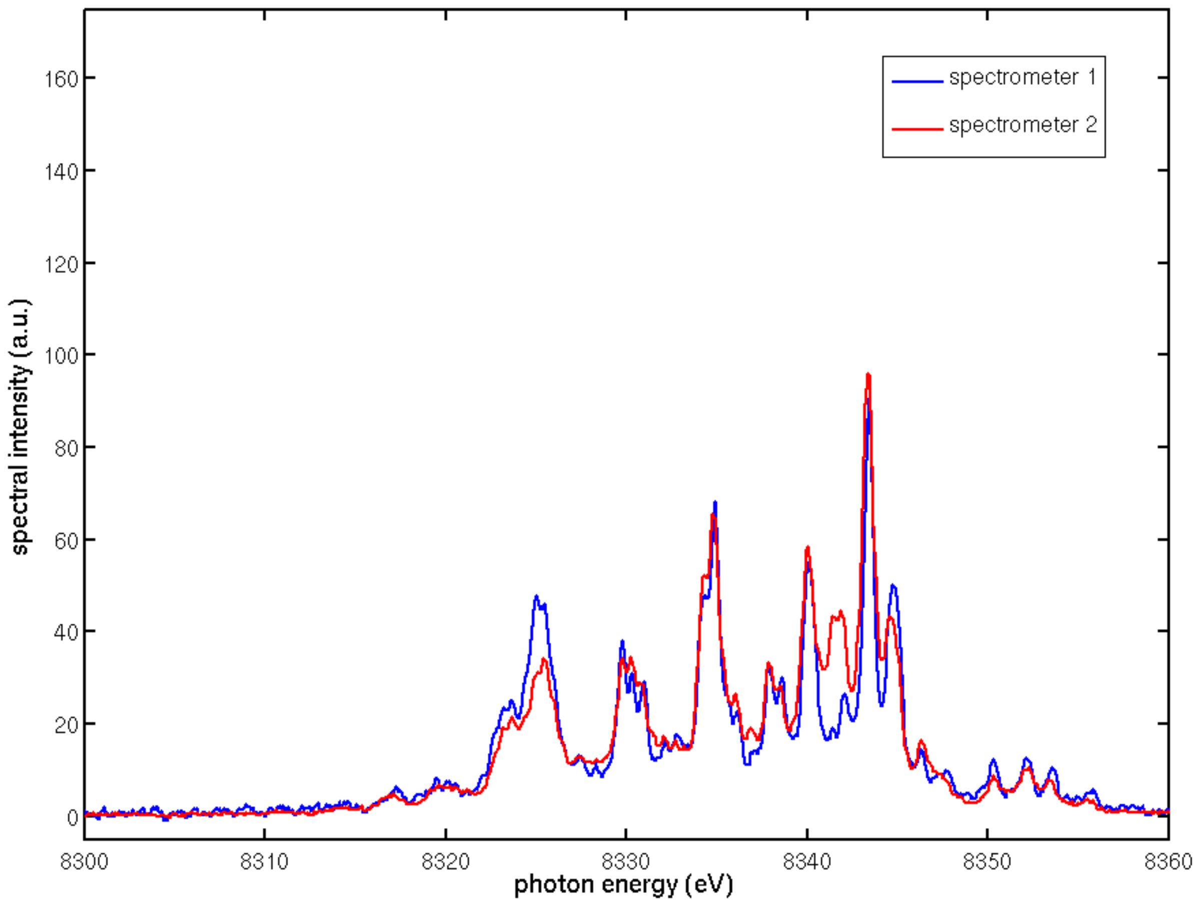

Fluctuations in the spectral (energy) domain of multiple SASE pulses from the LCLS x-ray FEL

Hard and Soft X-ray Self-Seeding at LCLS

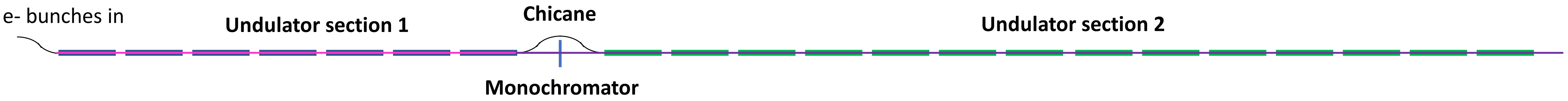

SASE is produced in Undulator Section 1

Coherent seed is amplified in Undulator Section 2

Hard X-ray Self-Seeding (HXRSS)
Monochromator = a thin Bragg crystal

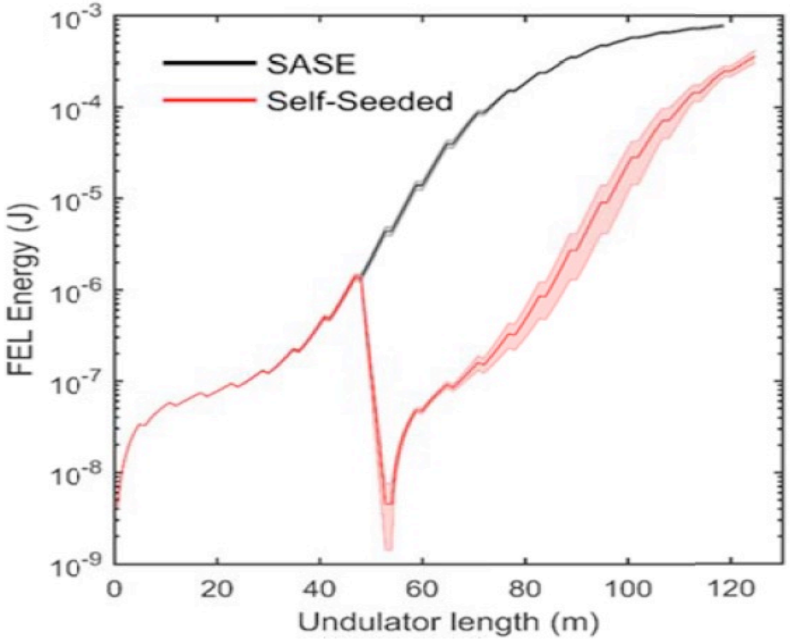

Soft X-ray Self-Seeding
Monochromator = a toroidal grating

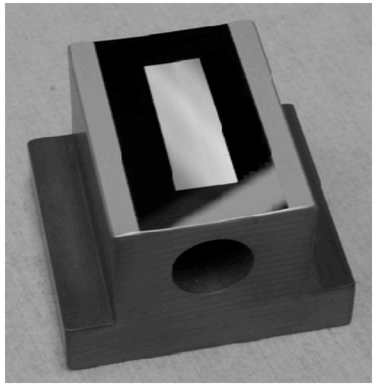

HXRSS reduces the SASE spectral width

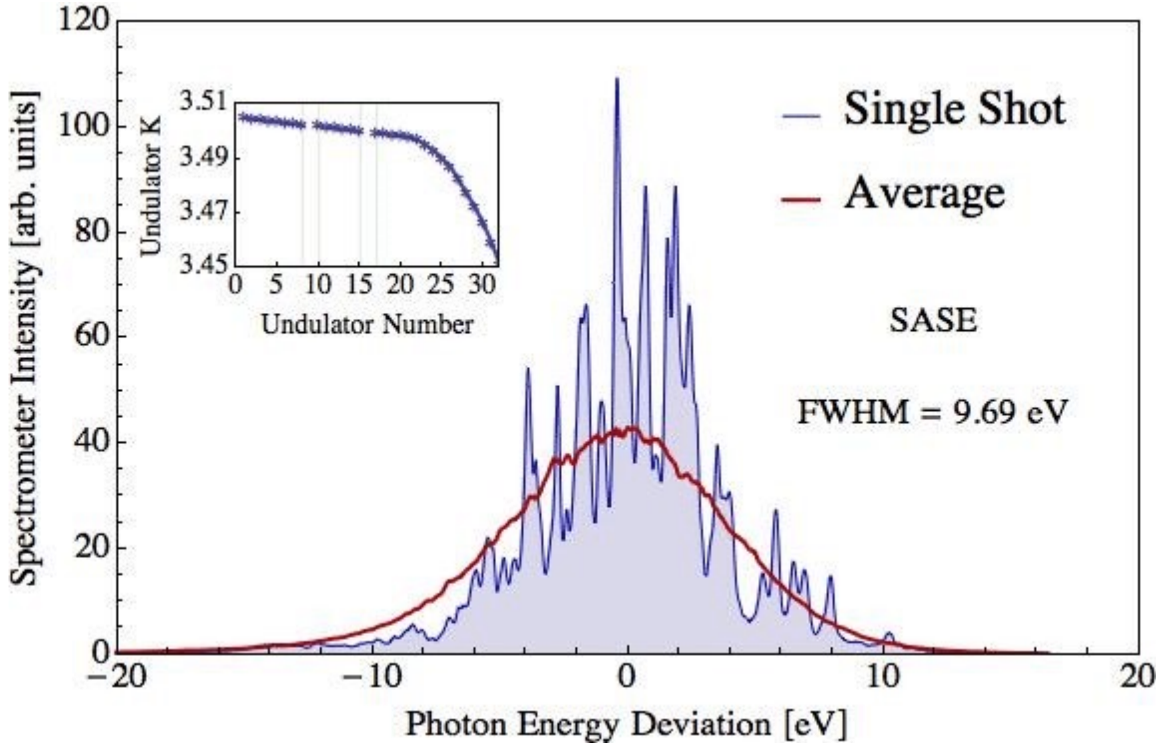

SASE spectra without self-seeding

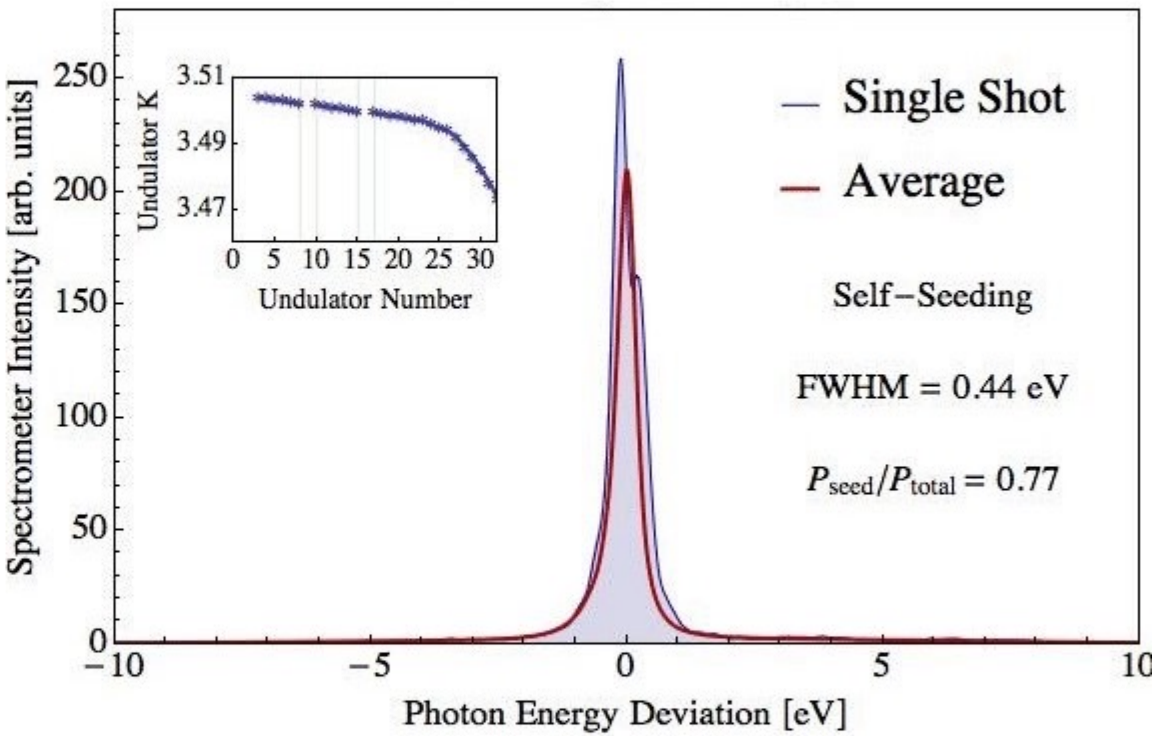

SASE spectra with self-seeding

C. Emma, UCLA Ph.D. Thesis (2017), https://escholarship.org/content/qt65p5d7h6/qt65p5d7h6.pdf

Bragg Law of Diffraction

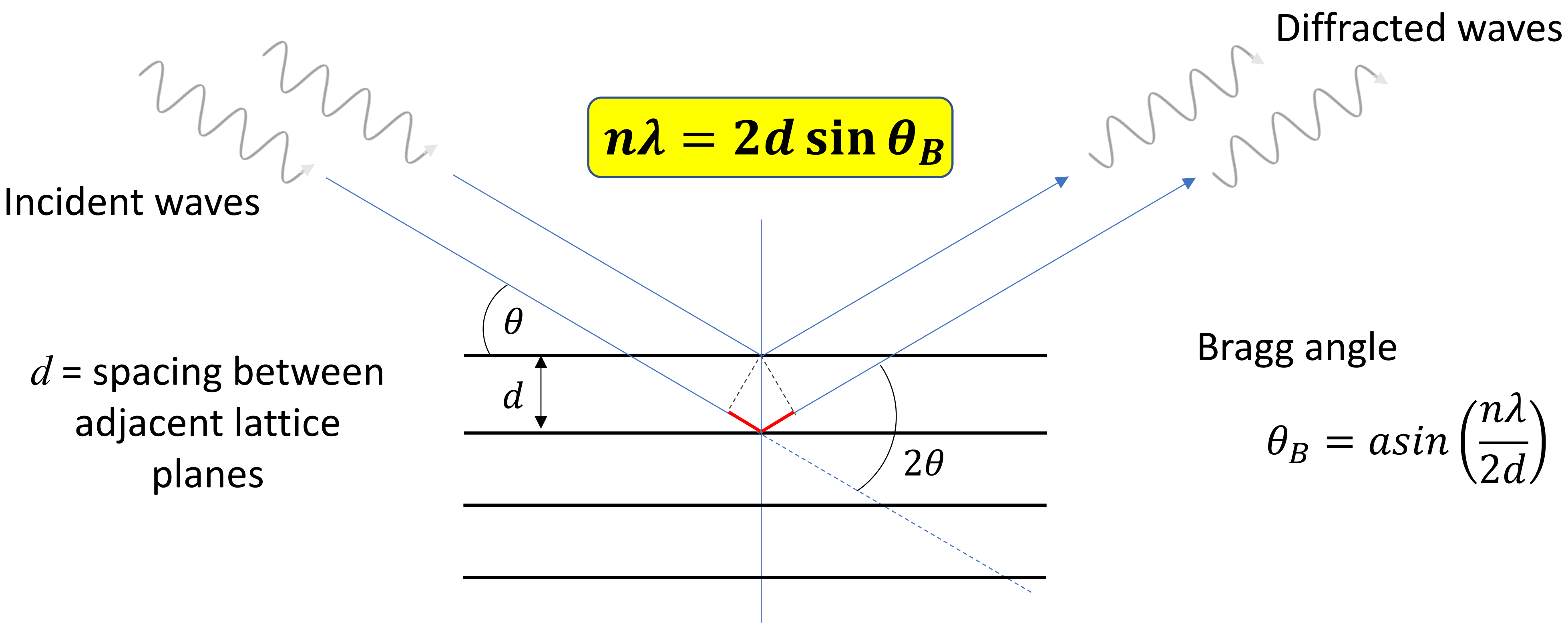

Bragg diffraction is an interference between two plane waves that are elastically scattered off lattice atoms with a spacing d between the adjacent lattice planes. The path length difference between two plane waves scattered off two adjacent lattice planes is shown in red. If the path length difference is a multiple of wavelengths, the scattered waves add constructively.

Rocking Curve & Darwin Width

The term "rocking curve" comes from a method in crystallography where the crystal is tilted by a small angle off the Bragg condition to produce a plot of diffracted x-ray intensity versus offset from the Bragg angle θ_B.

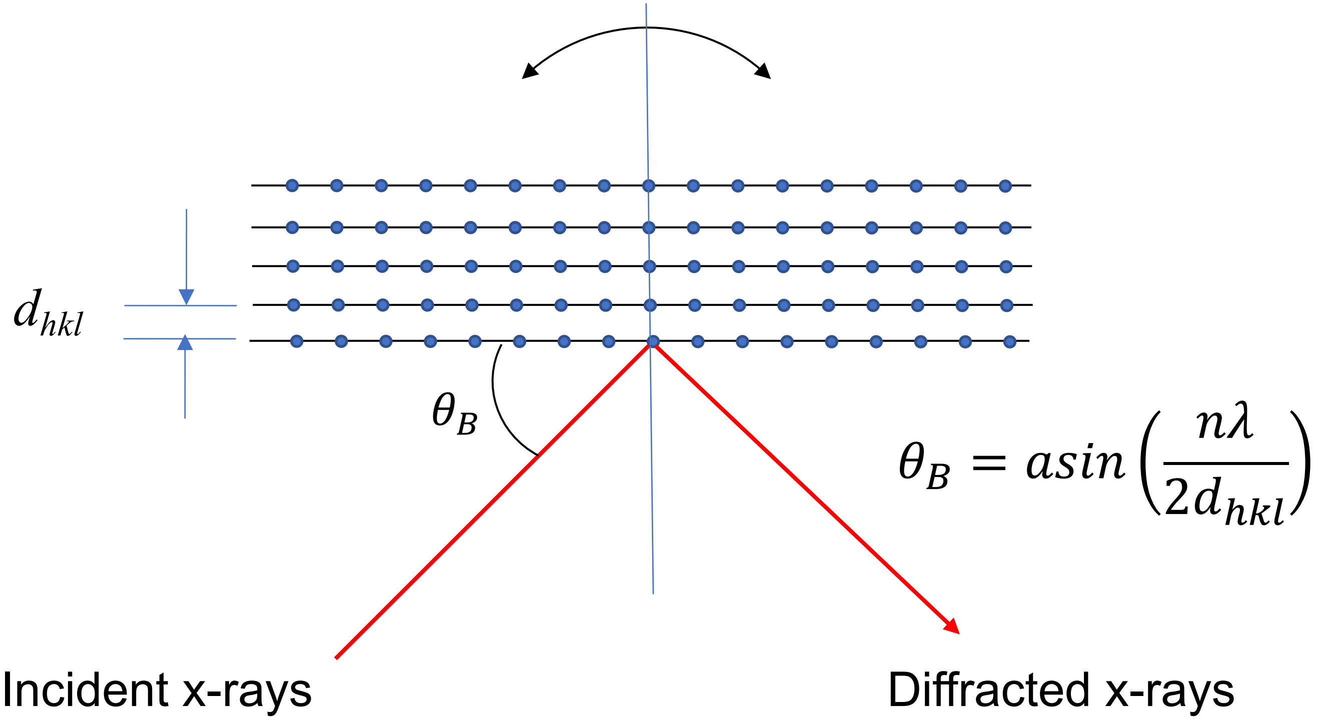

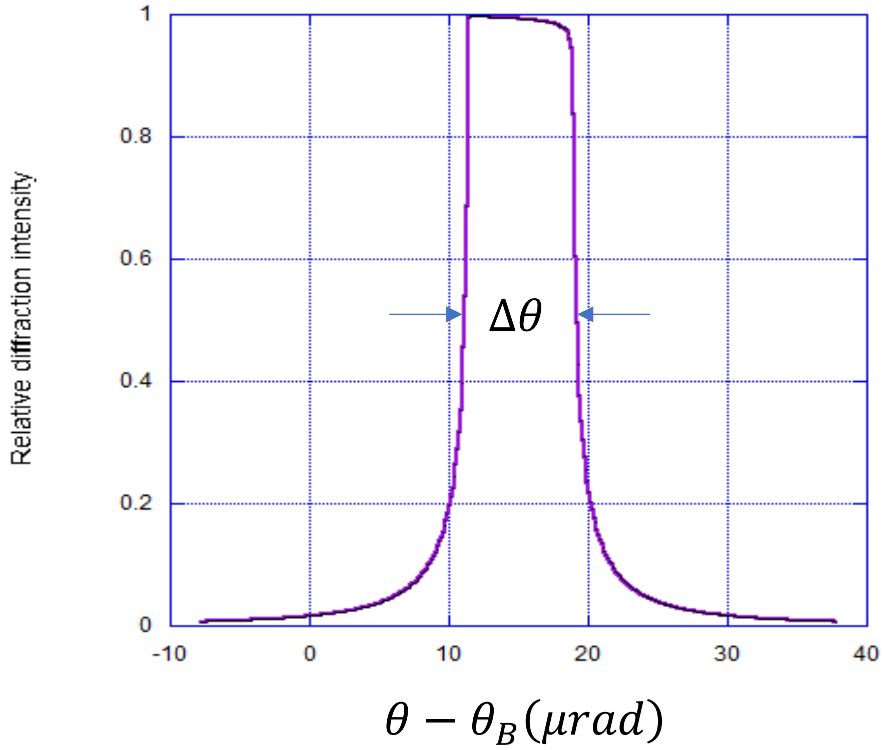

In symmetric Bragg diffraction, the incident and diffracted angles are the same as the Bragg angle θ_B.

Symmetric Bragg Diffraction Crystals

Bragg Crystal	d (Å)	Photon energy at 45° (keV)	Darwin Width at 45° (μrad)	Energy Width (eV)	Extinction Length (μm)	Absorption Length (μm)
Silicon (111)	3.1355	2.796	133.2	0.37	1.5	2.525
Diamond (111)	2.0593	4.257	59.4	0.25	2.2	54.79
Diamond (220)	1.2611	6.952	19.4	0.14	4.14	220.7
Diamond (311)	1.0755	8.152	8.80	0.072	7.78	591.2
Diamond (400)	0.8918	9.831	7.56	0.074	7.5	1074.2
Diamond (331)	0.8183	10.713	4.26	0.046	12.24	1413.9
Diamond (422)	0.7281	12.041	4.41	0.053	10.51	2055.5

Energy width

$$\Delta\varepsilon = \epsilon \, \Delta\theta \, cot\theta_B$$

Extinction length is the depth over which the atoms contribute to Bragg diffraction

Λ_H = Extinction length

Absorption length is the length over which the radiation intensity decreases to 1/e of the incident intensity due to absorption

λ_A = Absorption length

Hard X-ray Self-Seeding Experiments

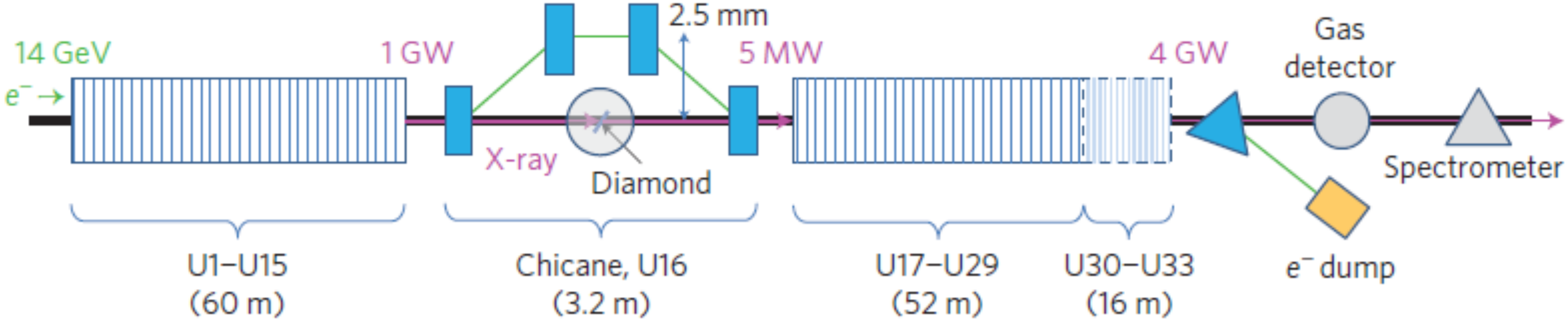

Chicane actions:

- wash out microbunching
- delay the electron bunch so it overlaps with one of the wake pulses
- offset the electron beam from the Bragg crystal

J. Amann et al., Nat. Photon. 6, 693 (2012)

How does HXRSS generate wake pulses?

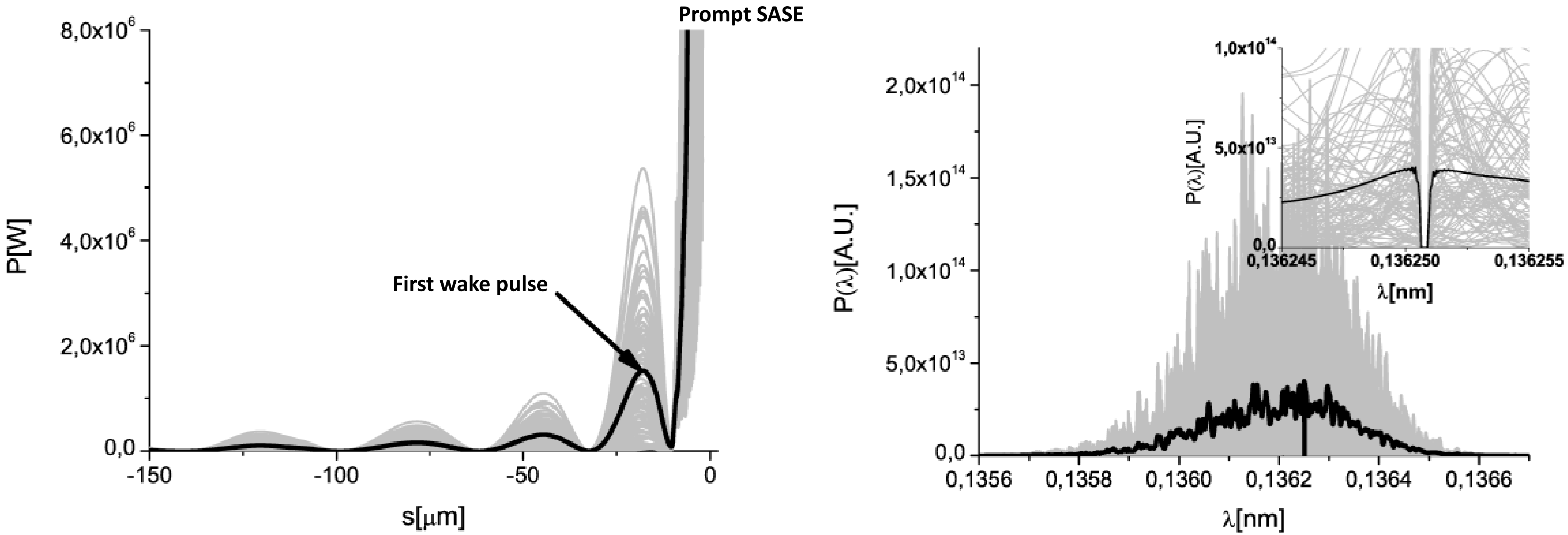

Bragg diffraction creates a spectral "notch" in the SASE spectrum. The Forward Bragg Diffraction (FBD) frequencies adjacent to the "notch" interfere constructively and destructively. In the time domain, this interference produces monochromatic wake pulses that follow the prompt SASE pulse.

L. Geloni et al., J. Mod. Opt. 58, 1391 (2011)

Monochromatic Wake Pulses

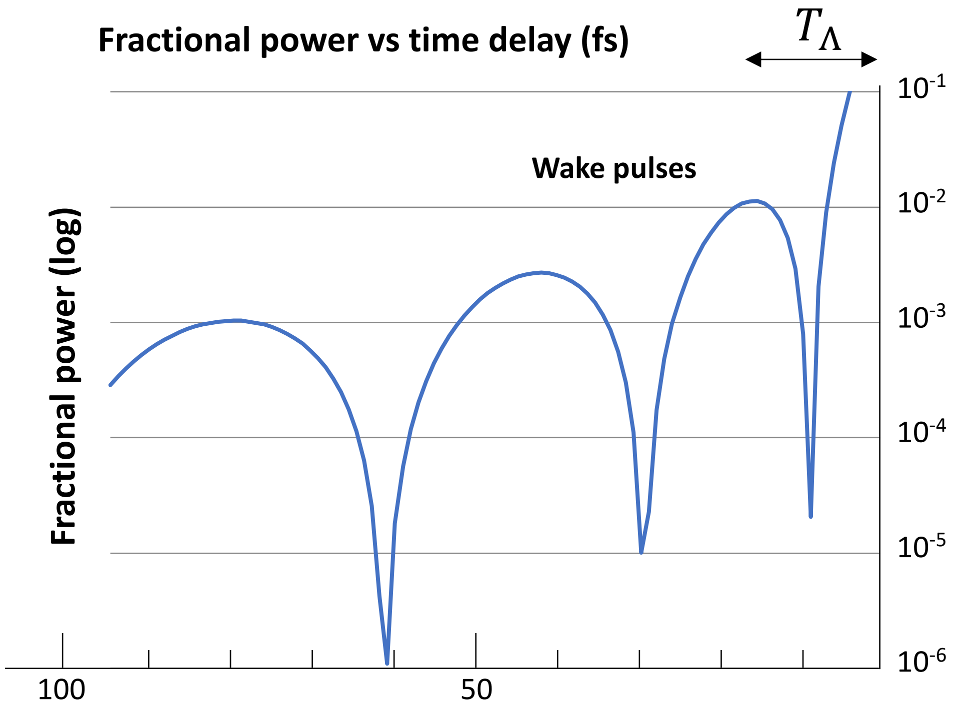

Central Energy $E_0 \approx \frac{1}{2}(E_{low} + E_{high})$

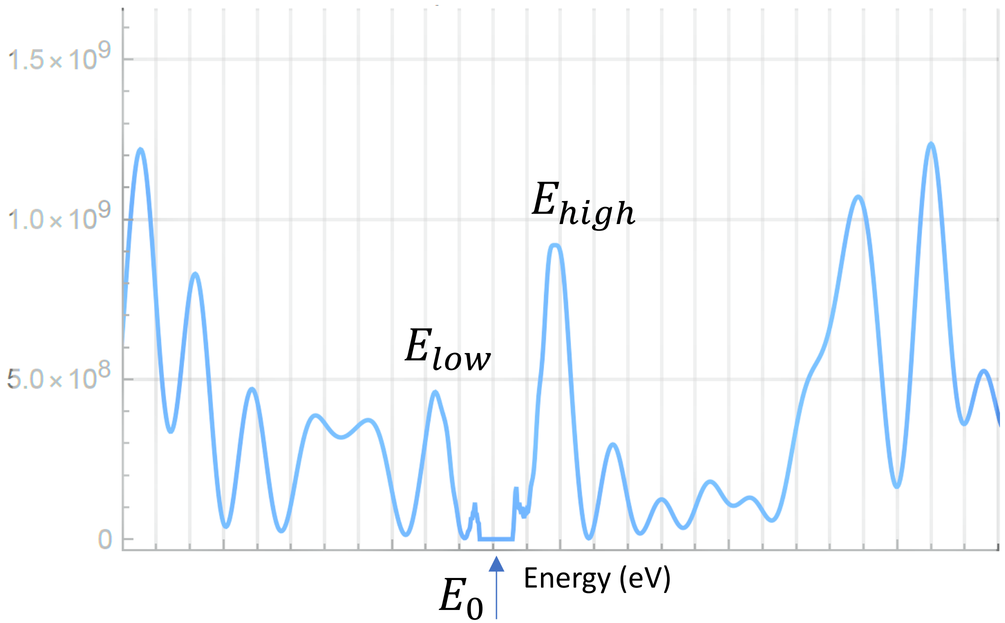

$$|G_{00}(t)|^2 \propto \left[\frac{1}{2T_0}\frac{J_1\left(\sqrt{\frac{t}{T_0}}\right)}{\sqrt{\frac{t}{T_0}}}\right]^2$$

First wake pulse delay

$$T_\Lambda = \frac{\Lambda_H}{2\pi\ c\ sin\theta_B}$$

Characteristic time

$$T_0 = \frac{\Lambda_H^2}{2\pi^2\ c\ d}$$

$\Lambda_H =$ Extinction length

$d =$ crystal thickness

Pathlength Delay & Offset in a Chicane

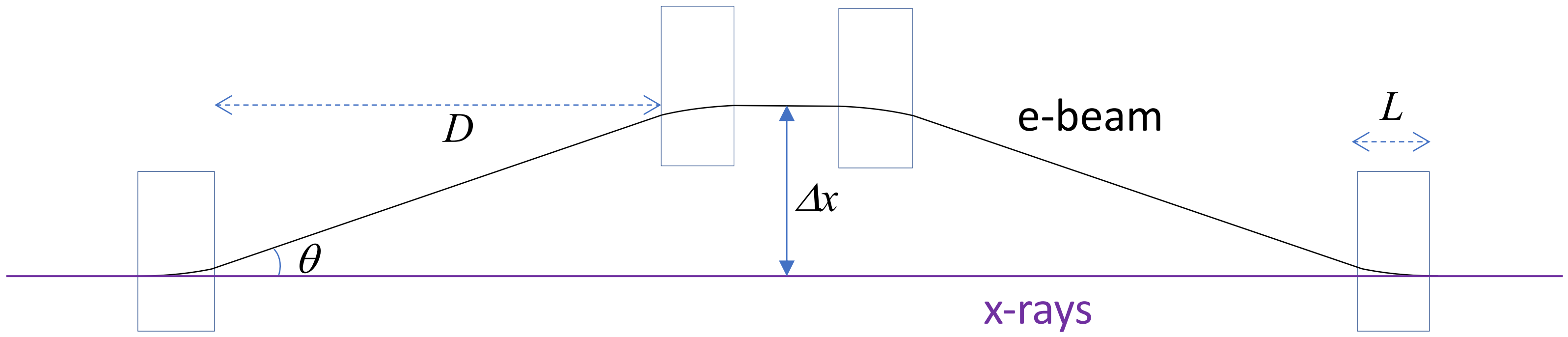

Difference between the electron and x-ray beam paths

$$\Delta L = \left(\frac{4}{3}L + 2D\right)\left(\frac{1}{cos\theta} - 1\right)$$

Chicane delay using small-angle approximation

$$\Delta L \approx \left(\frac{2}{3}L + D\right)\theta^2$$

Electron beam delay

$$\Delta t = \frac{\Delta L}{c} \qquad c = 0.3\ \mu m/fs$$

HXRSS Spectral Brightness Enhancement

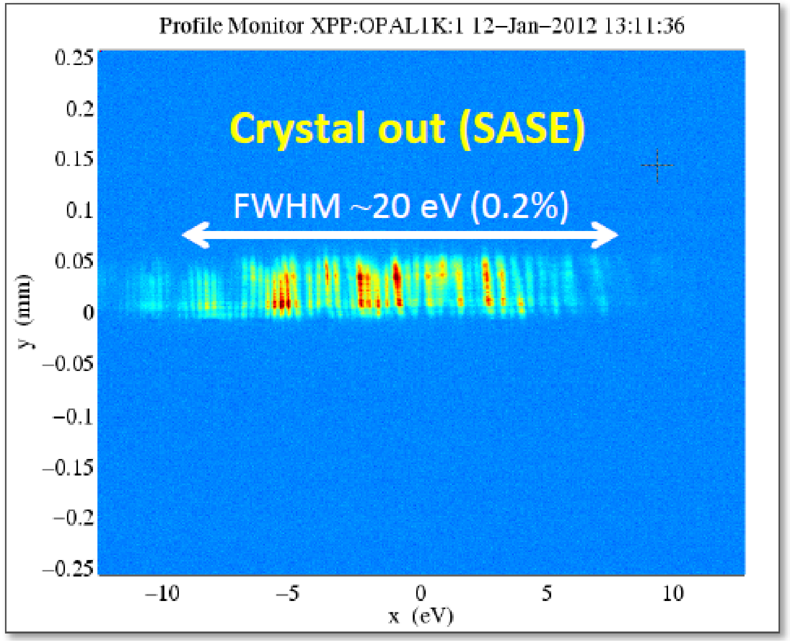

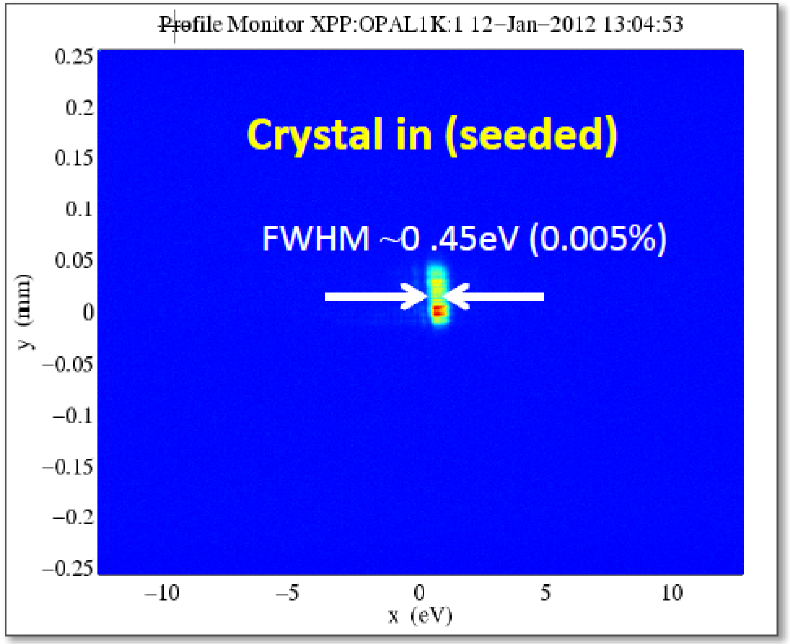

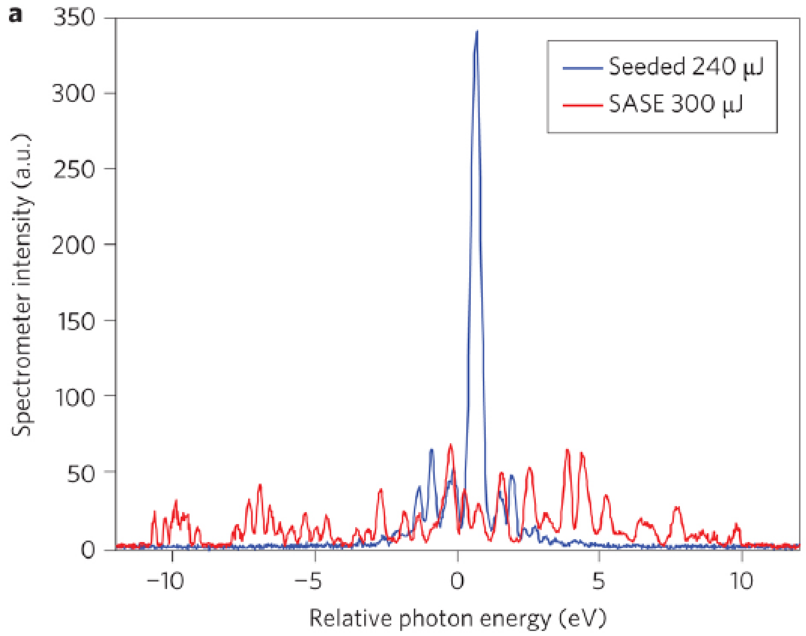

SASE relative BW

$$\frac{\Delta\omega}{\omega} \approx 1.5\rho \approx 2\times10^{-3}$$

HXRSS relative BW

$$\frac{\Delta\omega}{\omega} \approx 5\times10^{-5}$$

HXRSS brightness enhancement

$$\frac{\mathcal{B}_{SS}}{\mathcal{B}_{SASE}} \approx 30$$

Shot-to-shot Pulse Energy Fluctuations

Relative pulse energy fluctuation scales with $\sqrt{1/M}$

$$\frac{\sigma_W}{W} = \frac{\langle W - \langle W \rangle \rangle}{\langle W \rangle} \propto \sqrt{1/M}$$

where M = number of modes.

SASE $M \approx 160$ $\quad \frac{\sigma_W}{W} \approx 8\%$

HXRSS $M \approx 12$ $\quad \frac{\sigma_W}{W} \approx 30\%$

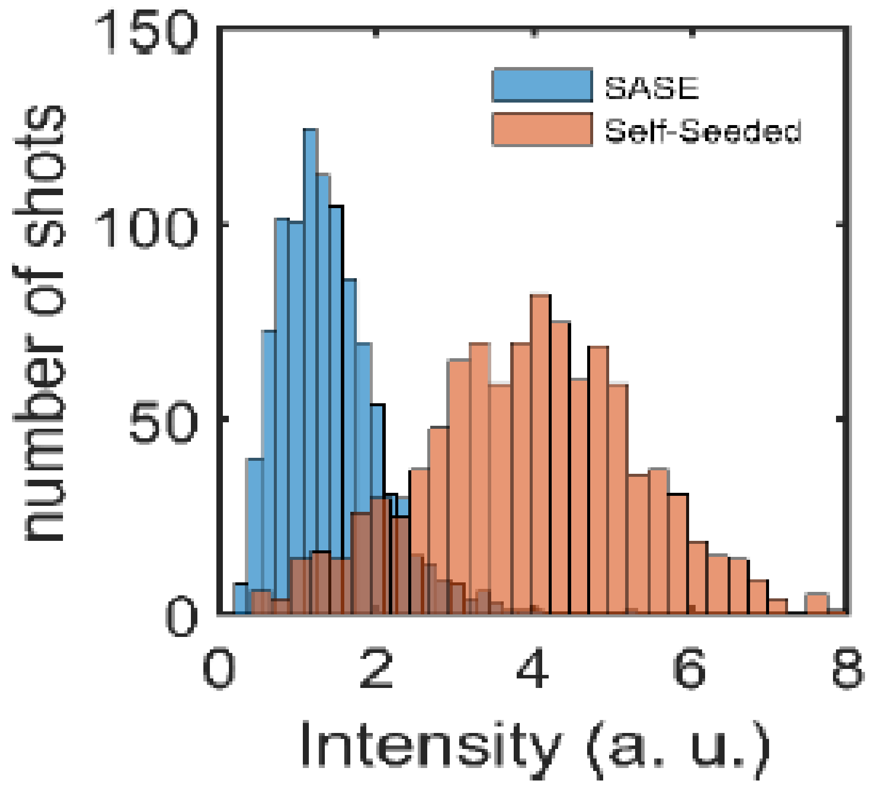

With the smaller M, HXRSS has much larger shot-to-shot pulse energy fluctuations than SASE

C.K. Min et al., J. Synchrotron Rad. 26, 1101 (2019)

Soft X-ray Self-Seeding

Soft X-ray Self-Seeding at LCLS

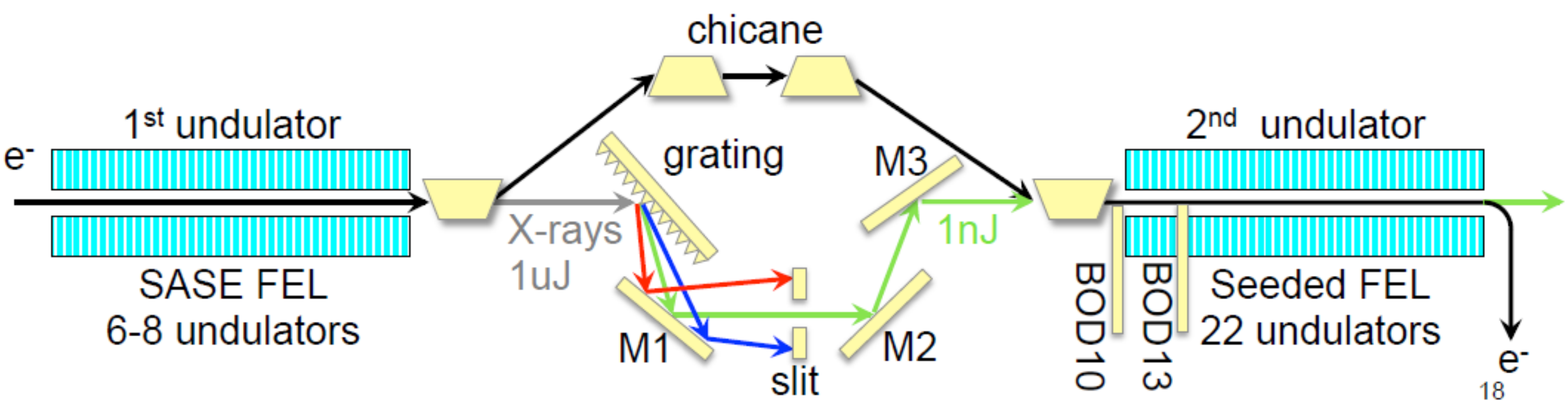

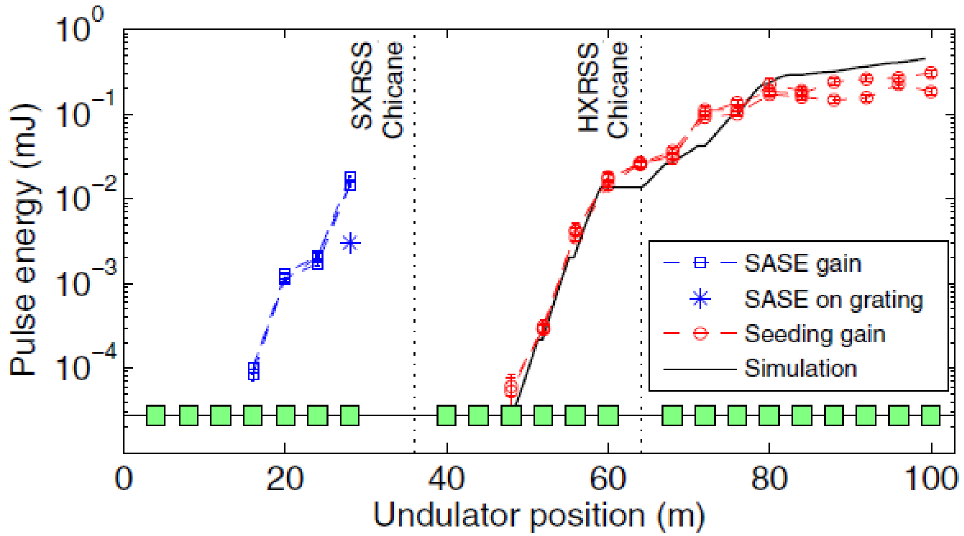

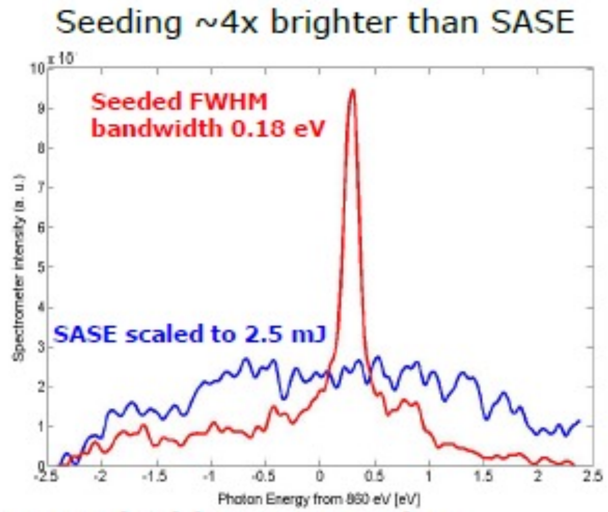

1.5-2 kA, 75-100 fs, 1-10uJ incident on grating

D. Ratner *et al.* Phys. Rev. Lett. **114**, 054801

SXRSS Diffraction Grating

Grating equation

$$n\lambda = d(\sin\alpha - \sin\beta)$$

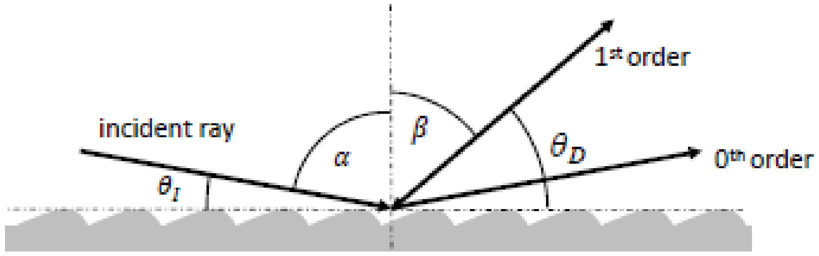

For LCLS SXRSS, the incident angle α is fixed at 89°

The exit angle β depends on the x-ray energy

Tuning x-ray energy by rotating M1 mirror about the pivot

Parameter	Symbol	Value	Unit
Line spacing	d	0.4452	μm
Linear coeff	$\Delta d/\Delta x$	$-6.621\text{x}10^{-7}$	
Groove height	h	15.6	nm
Grating efficiency @0.2 – 1.3 keV	$\eta_{Grating}$	3.77 - 0.58	%

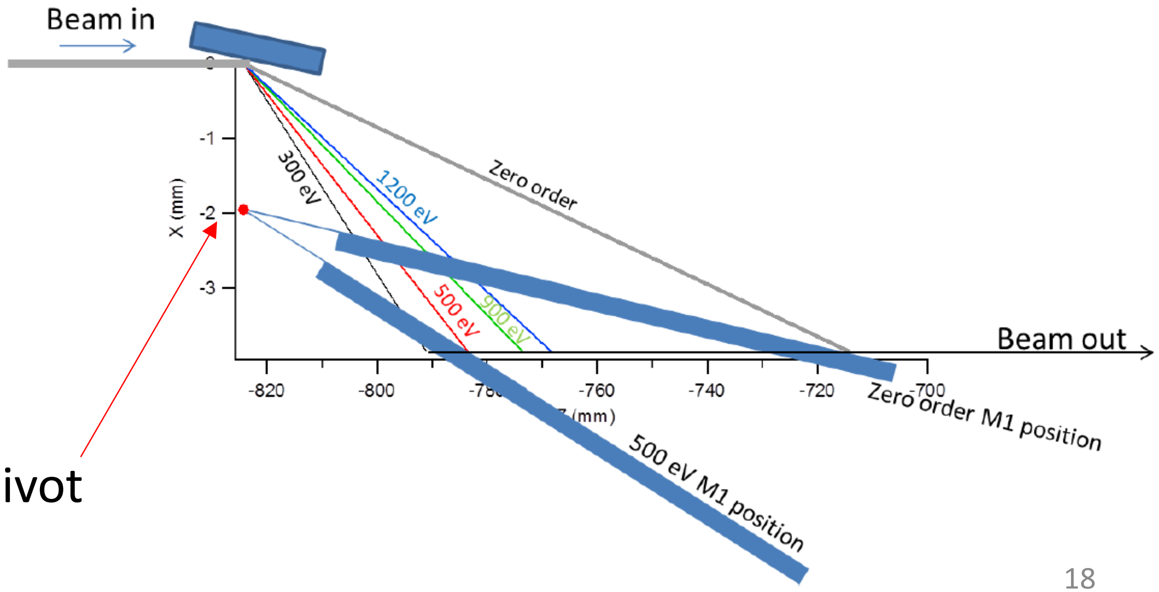

Focusing Property of the Toroidal Grating

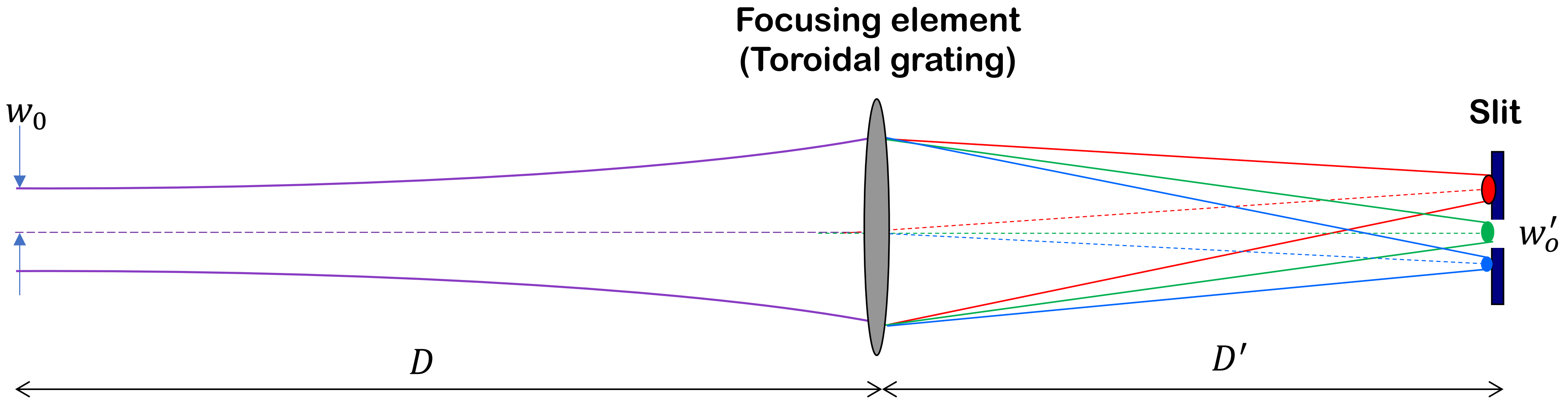

The toroidal grating focuses the x-ray beam on the slit and disperses different x-ray energies along the horizontal axis. The focusing property is energy dependent. At low x-ray energy, the SASE spectral width and w_o' are large, so the slit used to transmit the monochromatic seed with 1% bandwidth is also large. Therefore, the slit must have variable widths.

Photon energy	Vertical spot size (FWHM)	Horizontal spot size (1% SASE bandwidth)
(eV)	(μm)	(μm)
300	96	679
400	88	590
700	73	403
1000	65	284

SXRSS Delays (pathlength divided by *c*)

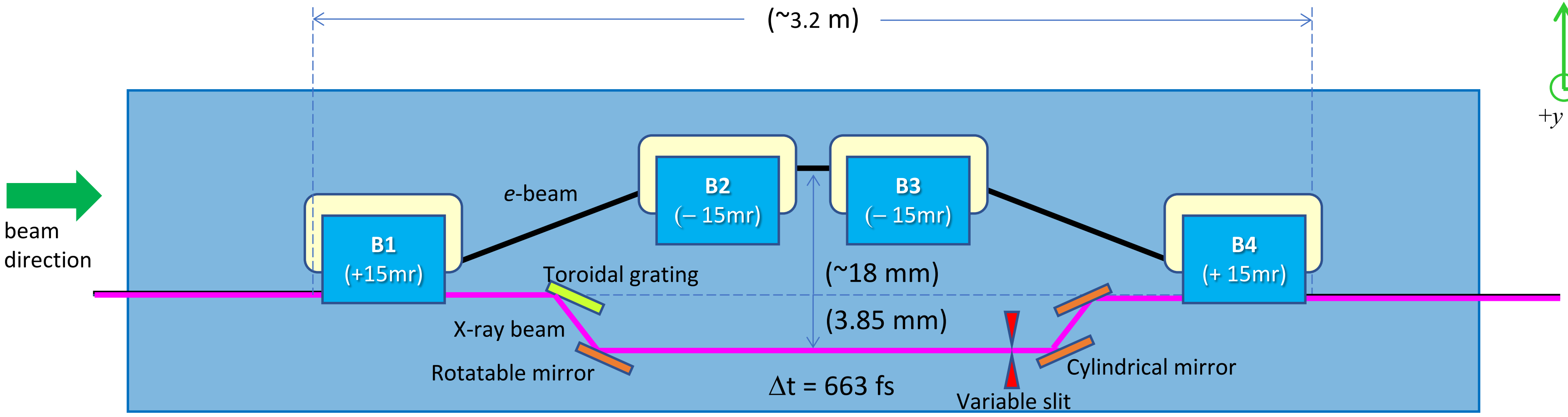

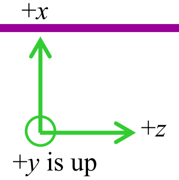

Unlike HXRSS, SXRSS must overlap the electron bunch with the main X-ray pulse

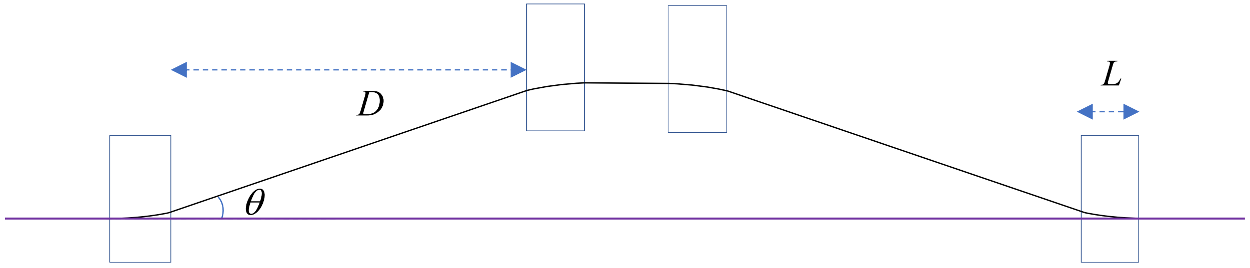

X-ray extra pathlength $\Delta L_r = 2\Delta x \cdot cot\phi$

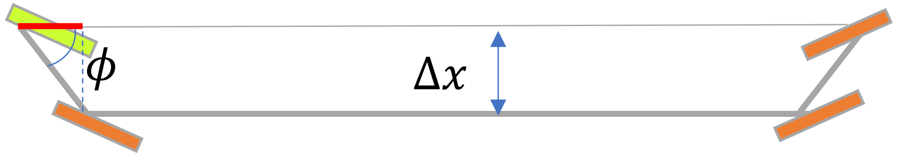

Electron extra pathlength $\Delta L_b = \left(\frac{2}{3}L + D\right)\theta^2$

SXRSS Performance at 1 keV

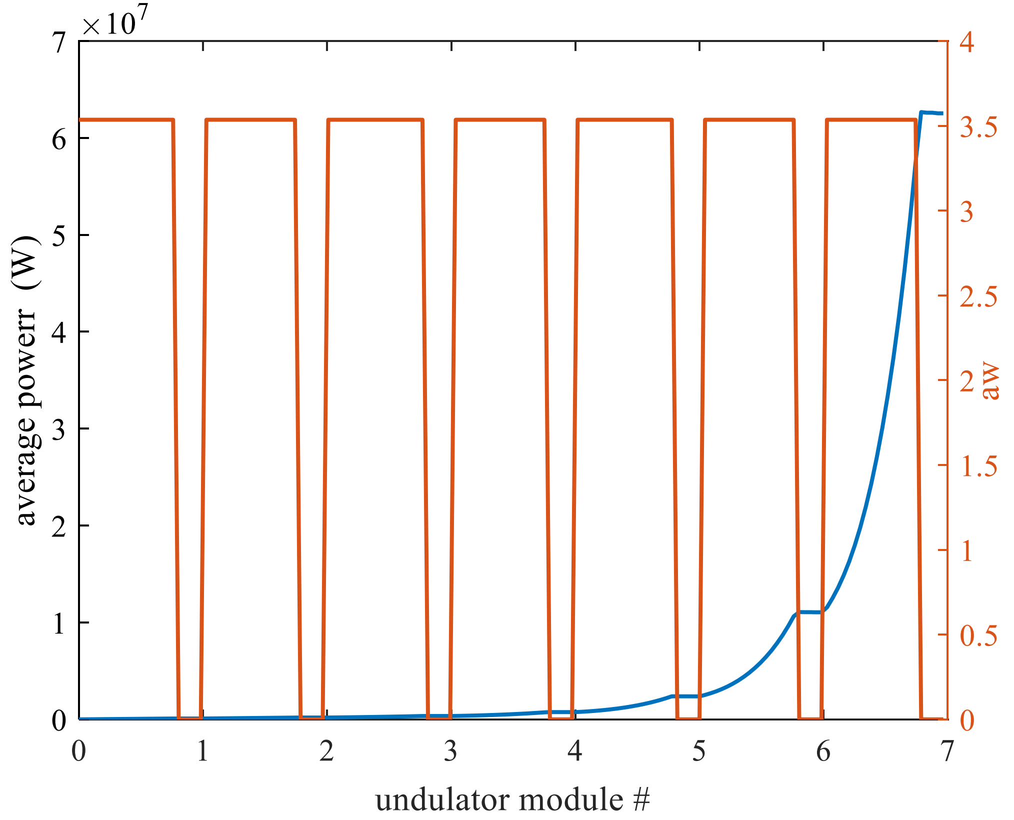

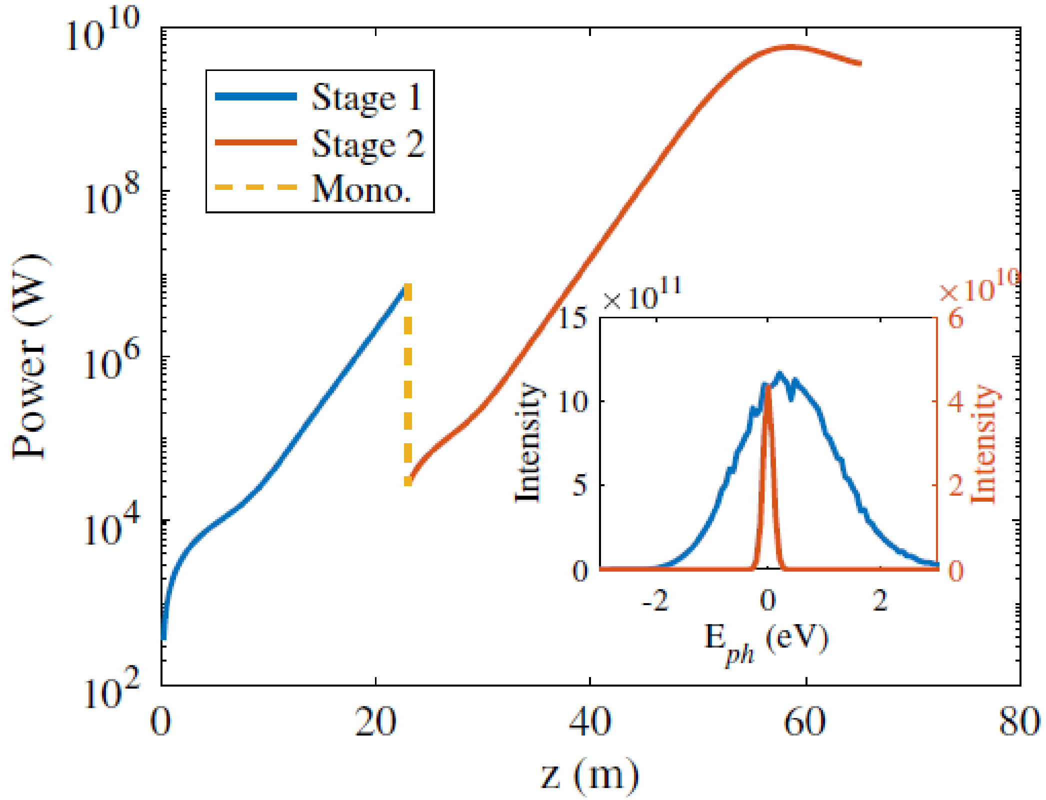

Max. seed power is 20 kW
(limited by grating damage)

Final SXRSS power is 8 GW

Regenerative Amplifier FEL

X-ray RAFEL with Bragg Reflectors

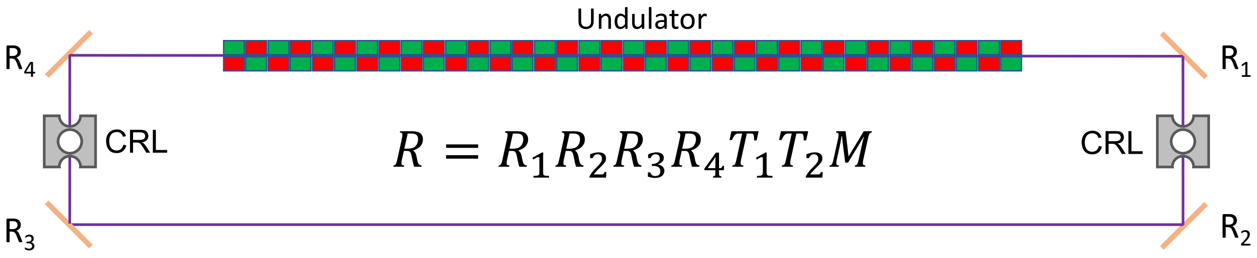

$$R = R_1 R_2 R_3 R_4 T_1 T_2 M$$

$R_1 R_2 R_3 R_4$ = Reflectivity of the Bragg reflectors within $\Delta\theta$

$T_1 T_2$ = Transmittivity of the two CRLs

M = Fraction of the return power that matches the FEL mode

RAFEL power in the n^{th} pass

$$P_n(z) = \frac{R P_{n-1}}{9} e^{\frac{z}{L_G}}$$

Bragg angle has to be slightly less than 45°

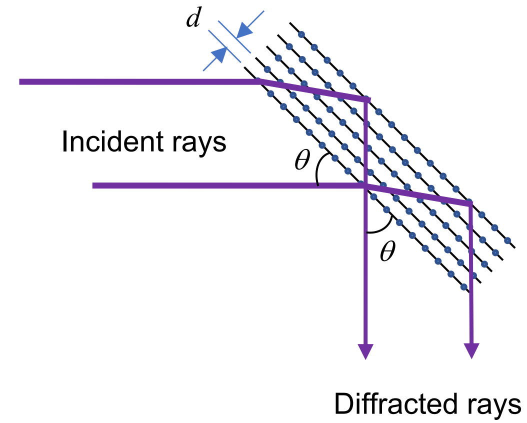

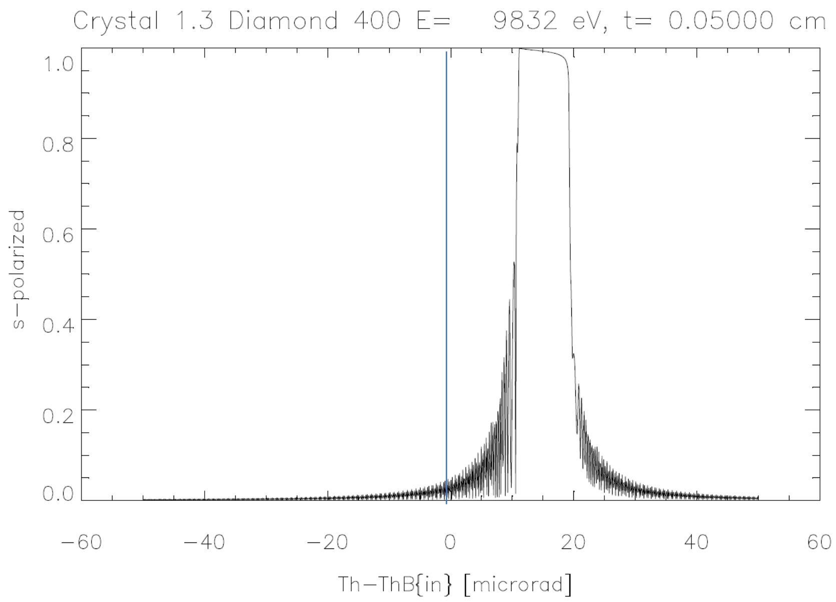

SASE, RAFEL and XFELO

	SASE	XRAFEL	XFELO
Peak Power	~10 GW	~50 GW	~100 MW
Average power	~100 W (at ~1 MHz)	10 W (at 10 kHz)	20 W (at ~1 MHz)
Spectral bandwidth	~10 eV	~0.1 eV	~1 meV
Pulse length	~ 1 – 100 fs	~ 20 fs	~ 1 ps
Stability	Poor	Excellent	Excellent
Longitudinal coherence	Poor	Excellent	Excellent
Transverse mode	Defined by gain-guiding	Defined by gain-guiding	Defined by the optical cavity

Characteristics of X-ray RAFEL

- Large single-pass gain
- High reflectivity in a narrow energy band
- Saturate in a few passes
- Output pulses = a train of fs pulses separated by the cavity roundtrip time
- Output X-ray beams have both temporal and spatial coherence
- Optics re-image X-ray beam from the undulator exit to the undulator entrance
- High gain + small optical feedback = Saturation

RAFEL Simulations with HXR Undulators

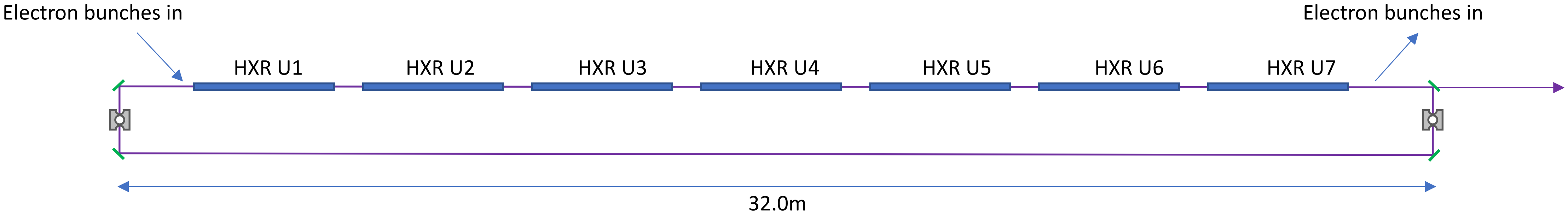

Electron beam energy-time

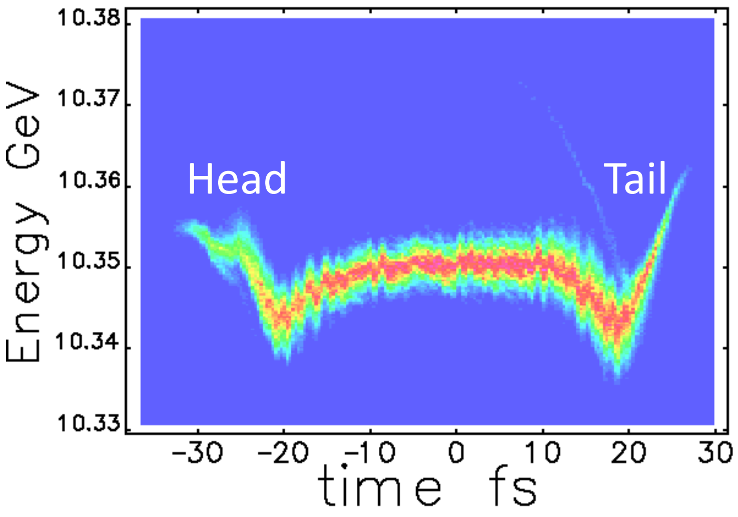

Current versus bunch coordinate

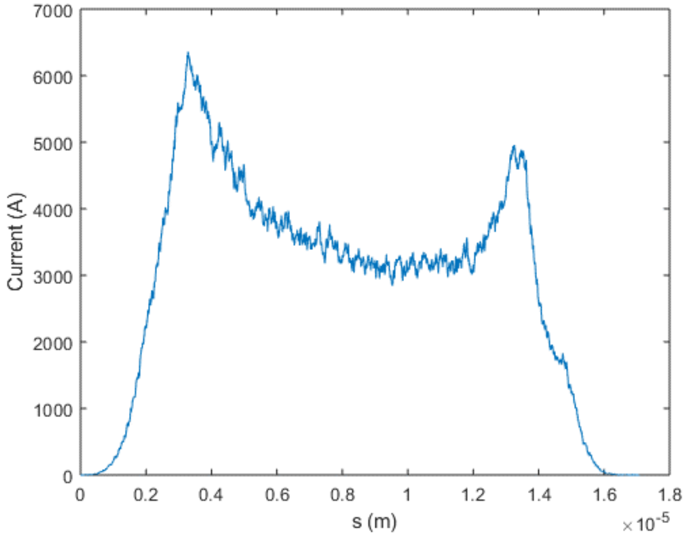

Radiation Electric Field Evolution

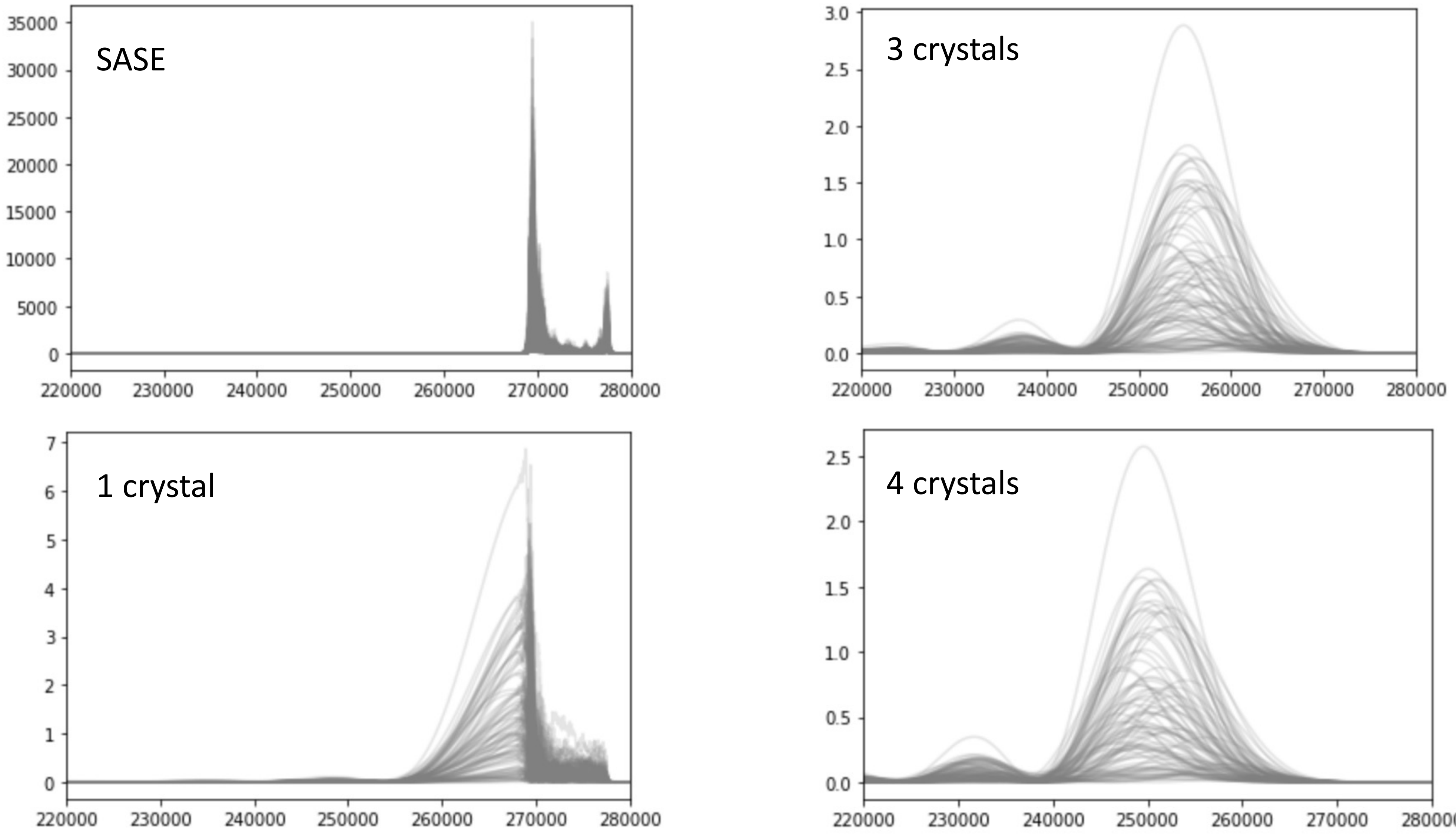

Expected Performance of XRAFEL

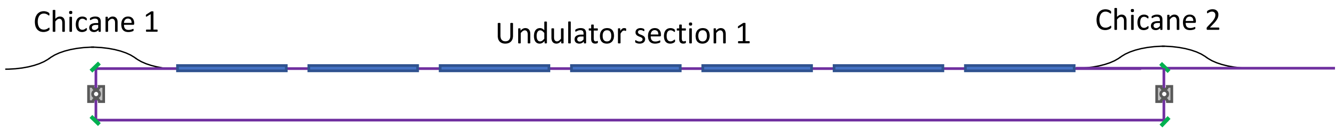

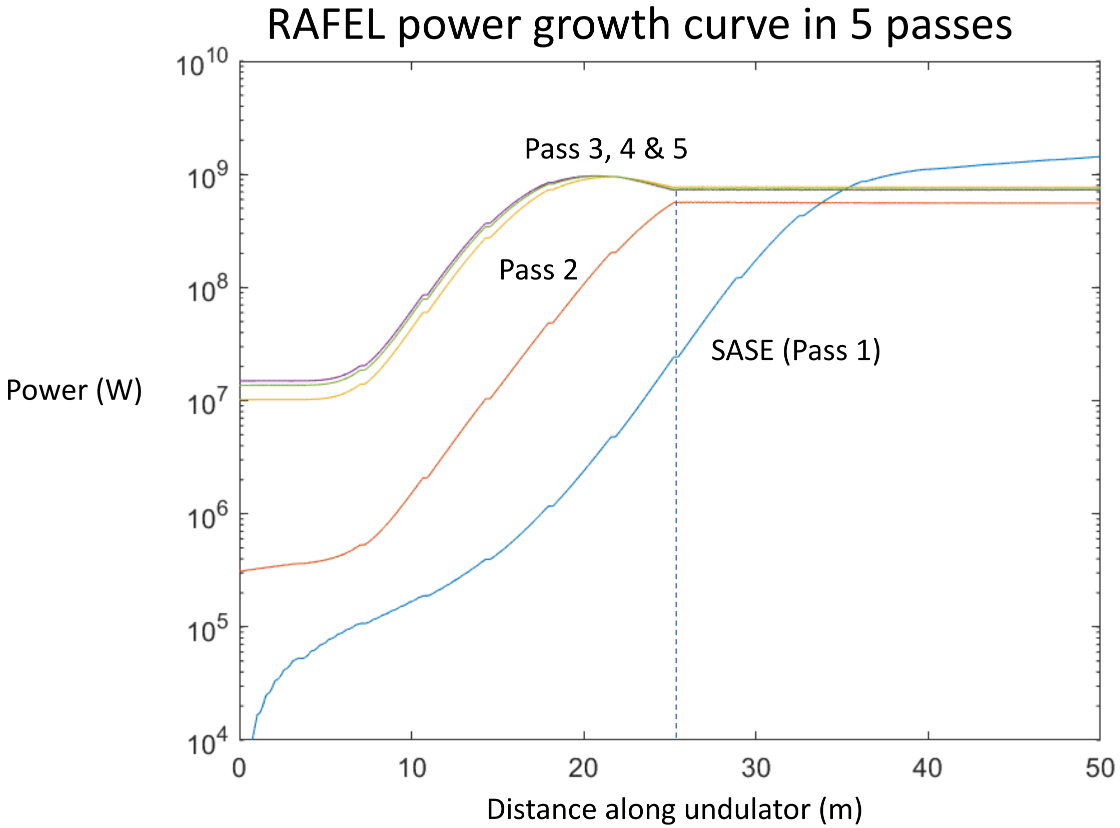

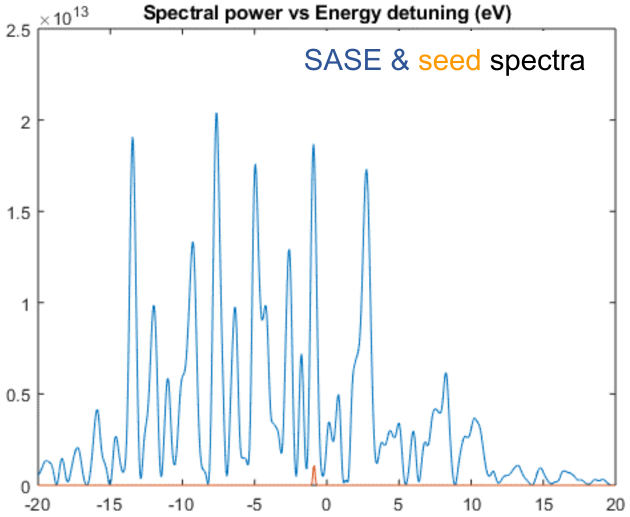

SASE in 1st Pass

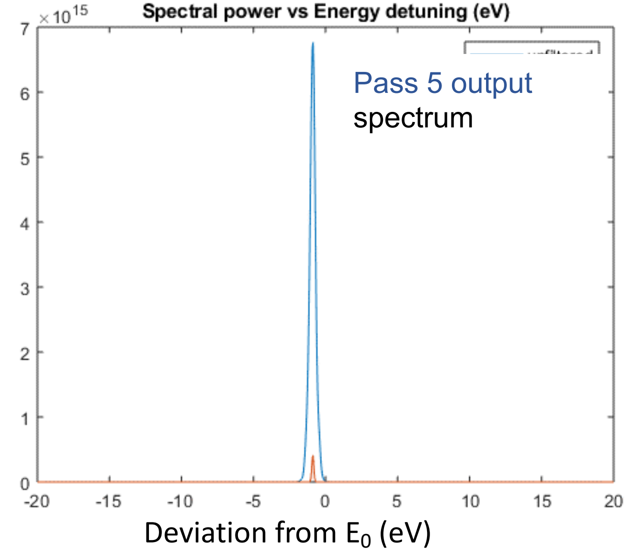

RAFEL in 5th Pass

Pass 1 (SASE) Filtering at 9.832 keV

Calculate the field spectrum (Fourier transform of radiation field versus time)

$$\mathfrak{I}(\omega) = \int_{-\infty}^{\infty} E(t)\, e^{-i\omega t} dt$$

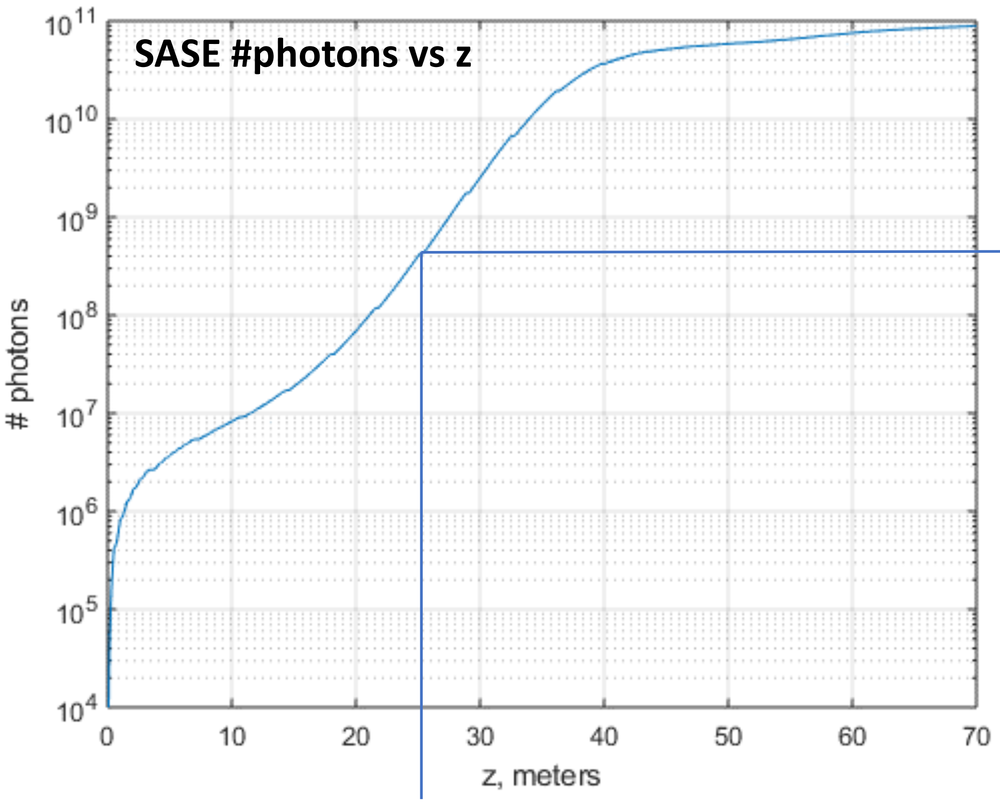

End of 7th HXU segment

$$\mathfrak{f}(\omega)\, \mathfrak{I}(\omega)$$

Field spectral filter

$$\mathfrak{f}(\omega) = F_0\, e^{-\frac{(\omega-\omega_0)^2}{2\sigma^2}}$$

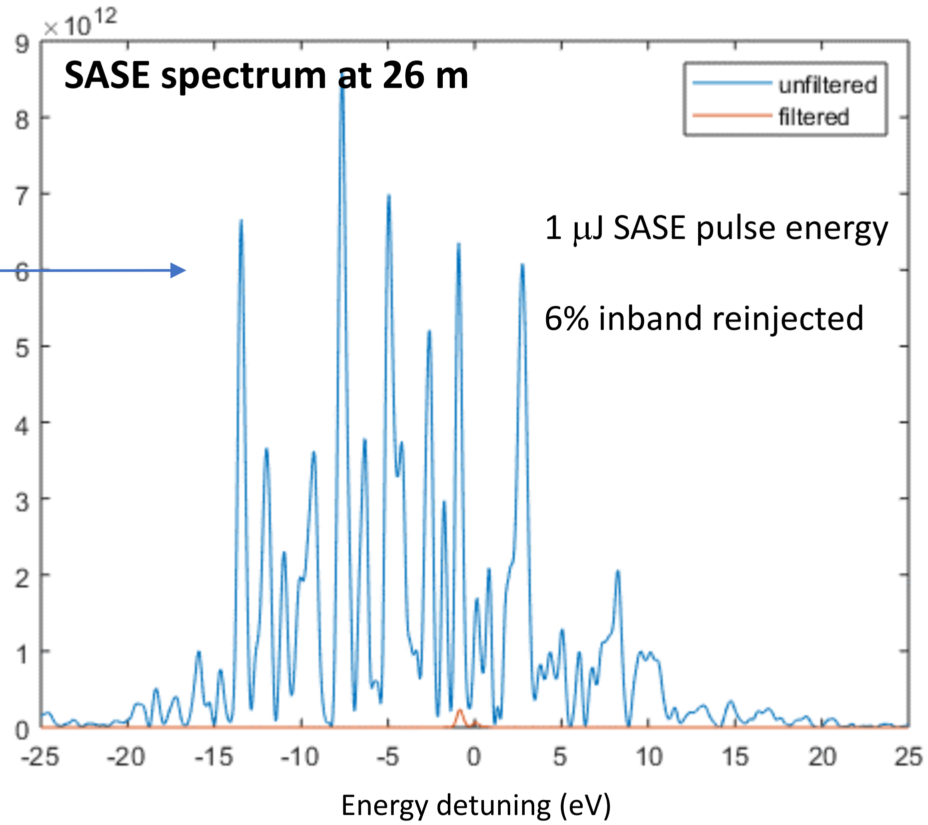

Pass 2 Number of Photons & Bandwidth

- 6% of the filtered SASE radiation at the end of the 7th HXU is reinjected
- Power grows to >10 GW in second pass
- Output spectrum has an rms bandwidth of 0.9 eV

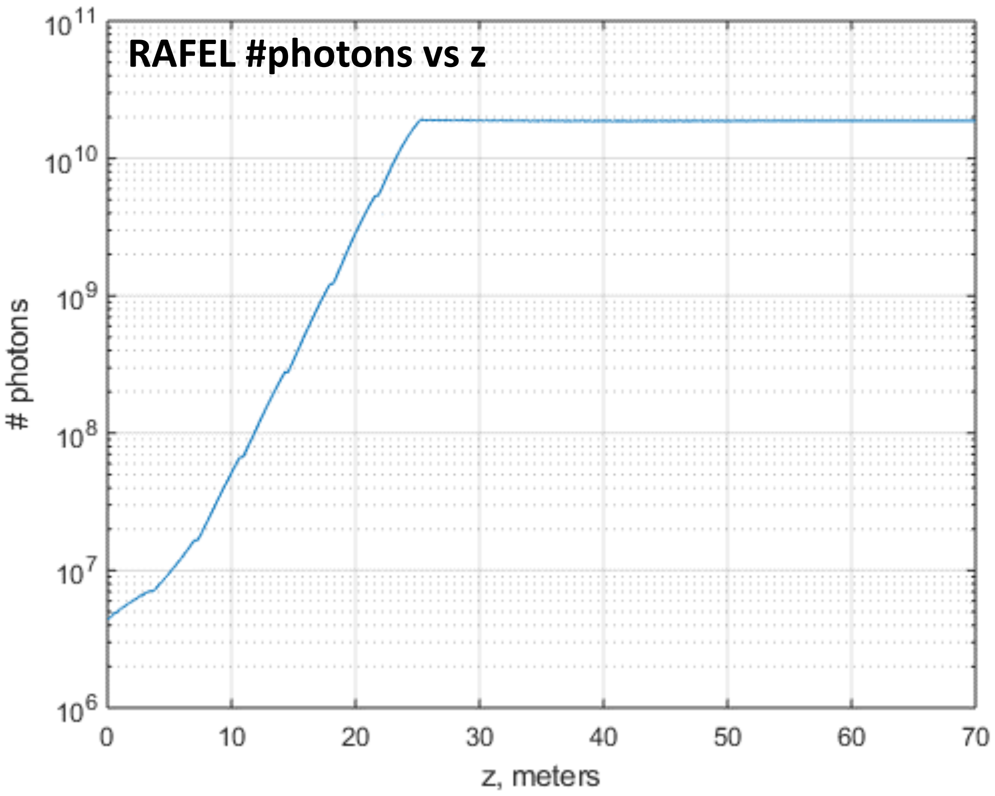

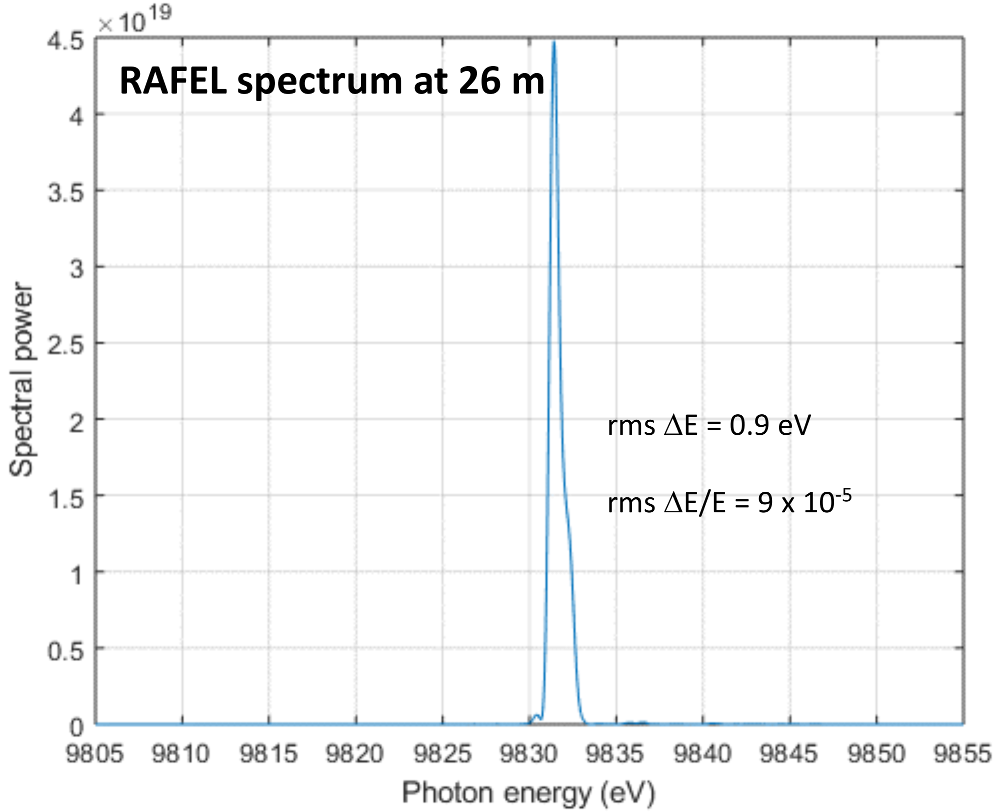

Pass 3 Number of Photons & BW

- 6% of the coherent radiation at the end of the 7th HXU in Pass 2 is reinjected
- Power saturates at the end of the 7th undulator
- Output spectrum has an rms bandwidth of 0.7 eV.

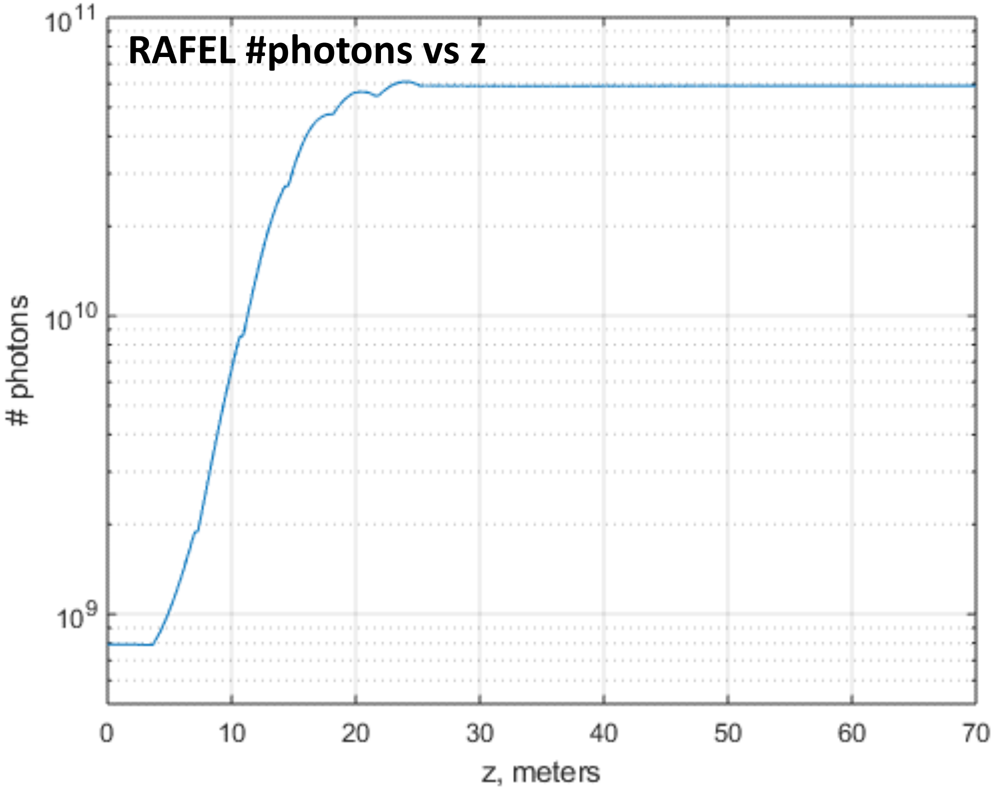

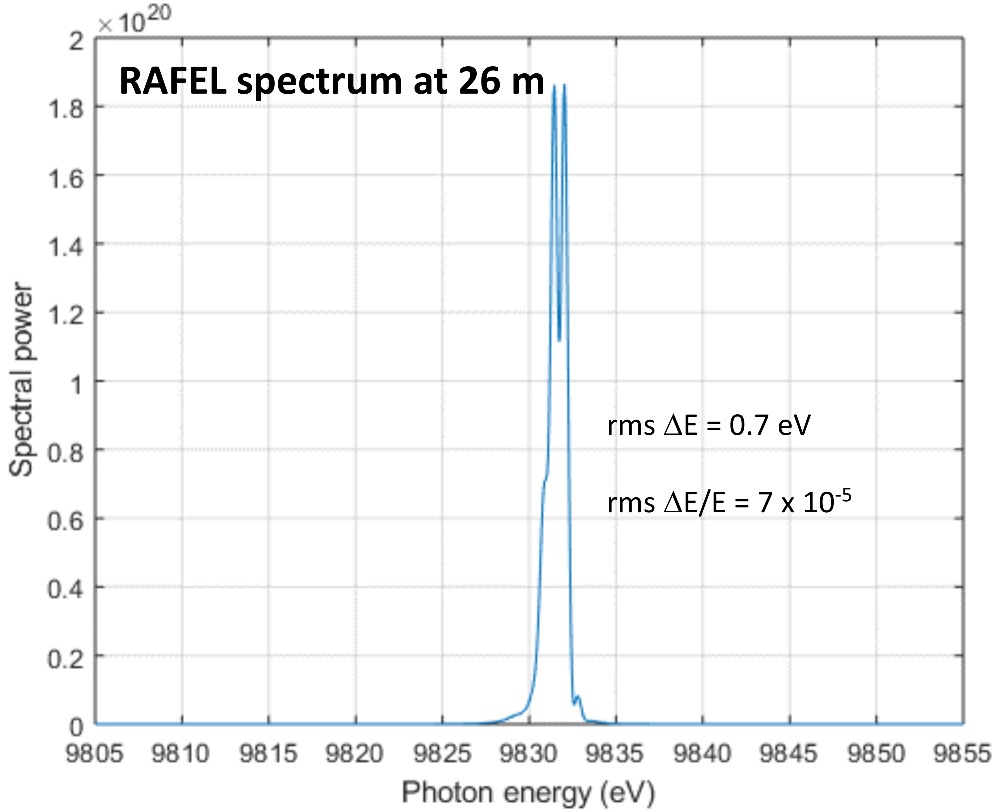

X-ray FEL Oscillator (XFELO)

X-ray FEL Oscillator (XFELO)

XFELO is the X-ray version of the FEL Oscillator
The first FEL (at 3.4 μm) was an FEL Oscillator

First Operation of a Free-Electron Laser*

D. A. G. Deacon,† L. R. Elias, J. M. J. Madey, G. J. Ramian, H. A. Schwettman, and T. I. Smith
High Energy Physics Laboratory, Stanford University, Stanford, California 94305
(Received 17 February 1977)

A free-electron laser oscillator has been operated above threshold at a wavelength of 3.4 μm.

Ever since the first maser experiment in 1954, physicists have sought to develop a broadly tunable source of coherent radiation. Several ingenious techniques have been developed, of which the best example is the dye laser. Most of these devices have relied upon an atomic or a molecular active medium, and the wavelength and tuning range has therefore been limited by the details of atomic structure.

Several authors have realized that the constraints associated with atomic structure would not apply to a laser based on stimulated radiation by free electrons.[1-5] Our research has focused on the interaction between radiation and an electron beam in a spatially periodic transverse magnetic field. Of the schemes which have been proposed, this approach appears the best suited to the generation of coherent radiation in the infrared, the visible, and the ultraviolet, and also has the potential for yielding very high average power. We have previously described the results of a measurement of the gain at 10.6 μm.[6] In this Letter we report the first operation of a free-electron laser oscillator.

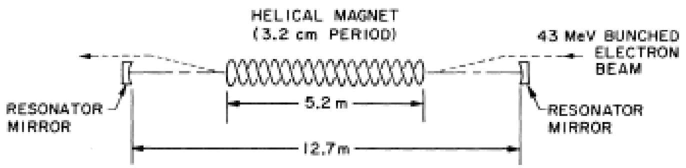

FIG. 1. Schematic diagram of the free-electron laser oscillator. (For more details see Ref. 6.)

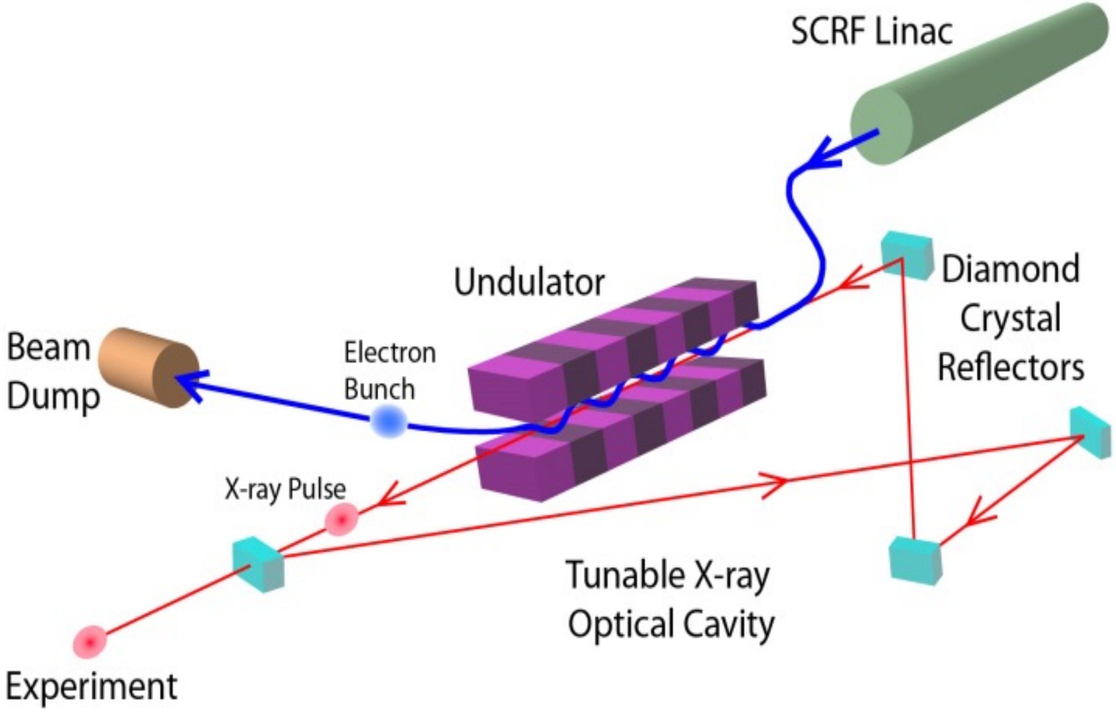

D.A.G. Deacon et al., Phys. Rev. Lett. 38, 892 (1977)

K.-J. Kim et al., Phys. Rev. Lett. 100 244802 (2008)
Yu. Shvyd'ko et al., Nature Photonics 5 (2011) 539

FEL Oscillator Glossary

- Small-signal gain (G_{SS})

$$P_{out} = (1 + G_{ss})P_{in}$$

- Saturated gain = Cavity loss

$$P_{out} = (1 + L)P_{in}$$

- Optical cavity

$$L_{cav} = \frac{c}{f_b}$$

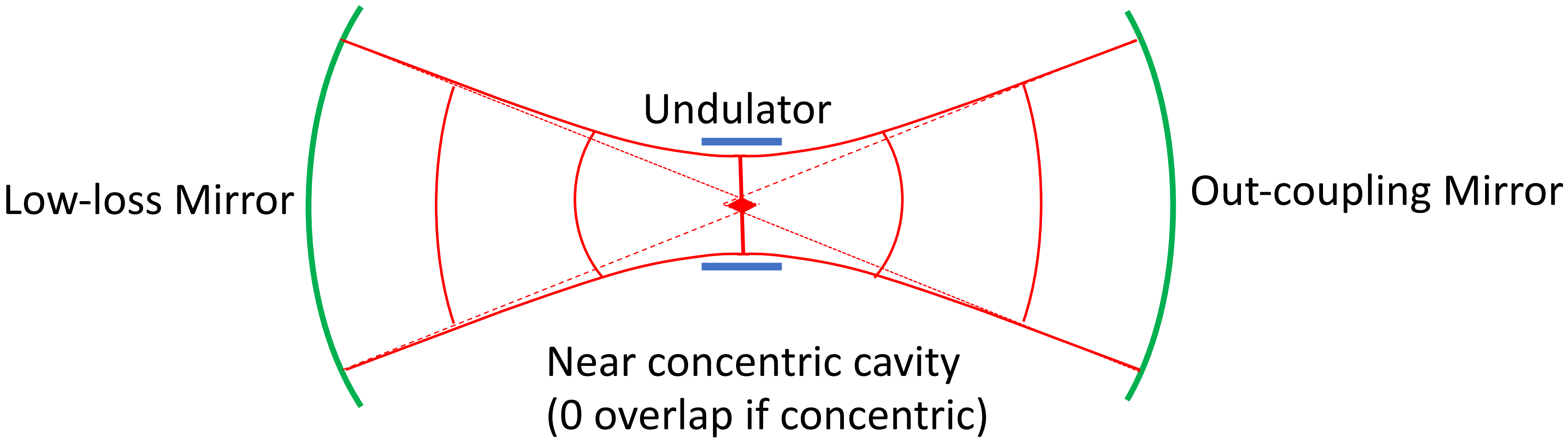

- Cavity loss = Out-coupling + Mirror absorption + Diffraction

Small-Signal Gain

The small-signal gain peaks at a longer wavelength than the resonant wavelength.

$G_{ss}(\Delta)$

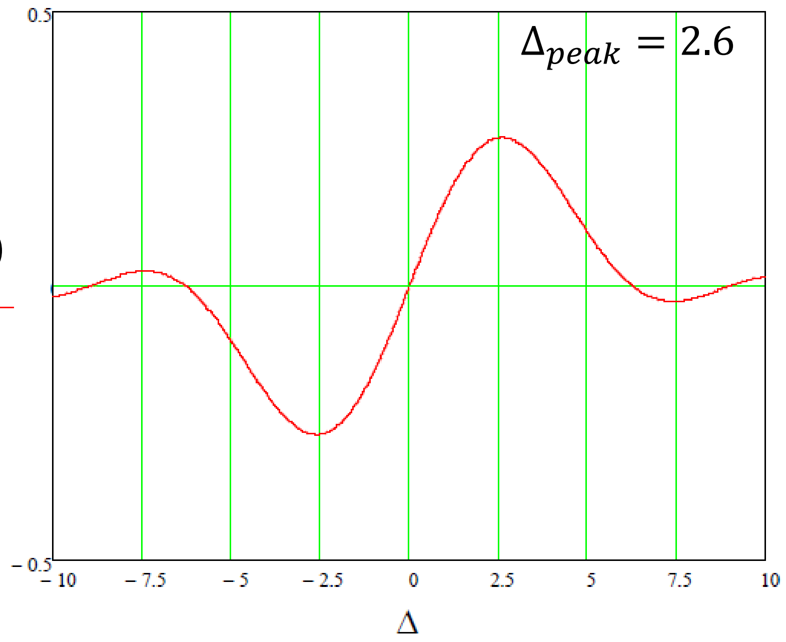

$$G_{ss}(\Delta) = \frac{4(4\pi\rho N_u)^3}{\Delta^3}\left(1 - \cos\Delta - \frac{\Delta}{2}\sin\Delta\right)$$

Detuning $$\Delta = \pi N_u \eta = 2\pi N_u \frac{\Delta\lambda}{\lambda}$$

At the peak of the gain curve

$$\Delta = 2.6 \Longrightarrow G_{ss} = (0.0675)\, 4(4\pi\rho N_u)^3$$

Large-Signal Gain & Saturation

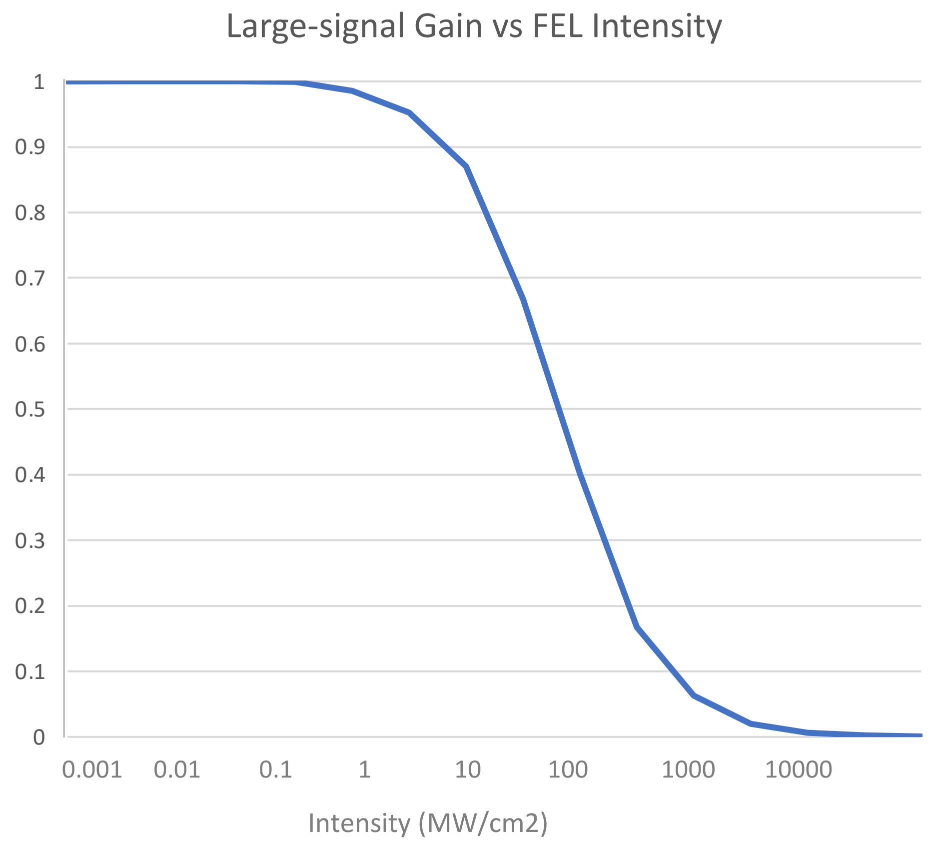

Gain decreases with intracavity FEL intensity

$$G(I) = \frac{G_{ss}}{1 + \left(\frac{I}{I_{sat}}\right)}$$

Saturated intracavity intensity

$$I_{sat}\left[\frac{MW}{cm^2}\right] \approx 100\pi \left(\frac{\gamma}{N_u}\right)^4 \frac{1}{\left(\lambda_u[cm]\widehat{K}\right)^2}$$

FEL Oscillator Power Growth in Many Passes

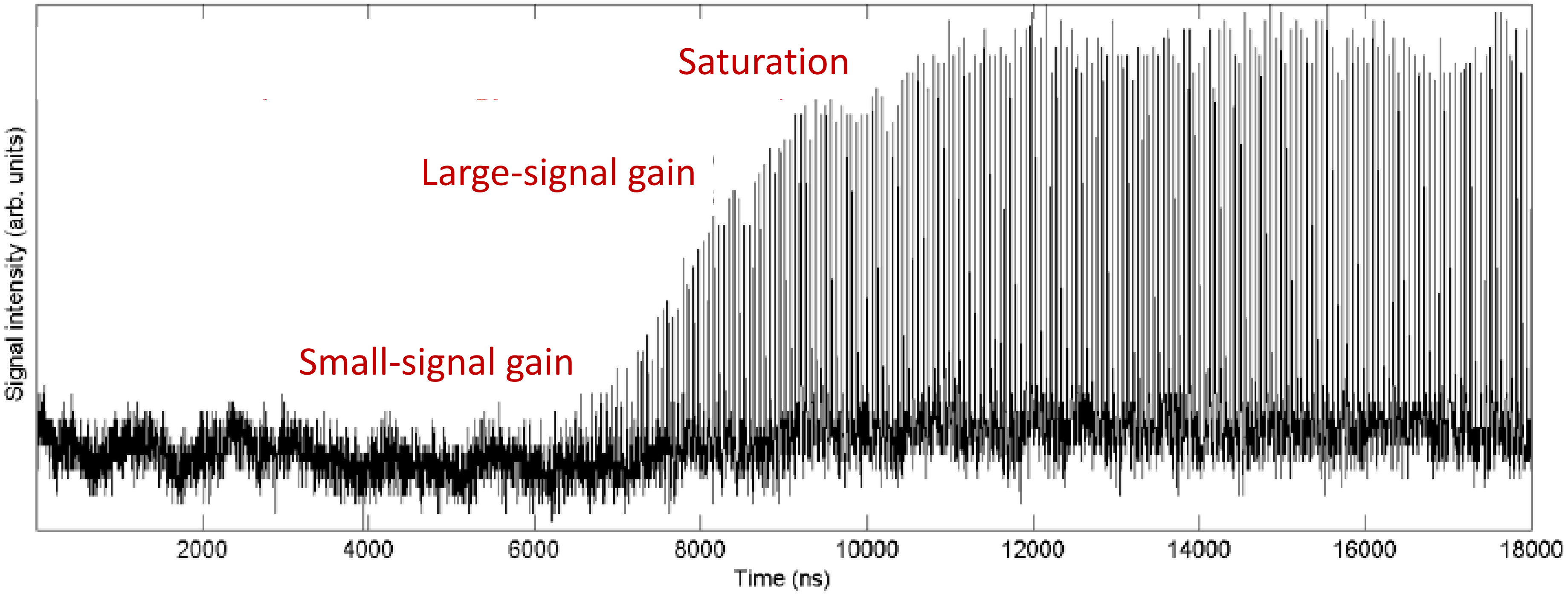

The small-signal gain is the highest single-pass gain
Gain decreases as the optical power grows (large-signal gain)
FEL saturates when intracavity power reaches the maximum

Maximum intracavity power

$$P_{in} = \frac{1}{2N_u} P_b$$

Courtesy of Andy Wolski, Introduction to FEL, CERN Accelerator School

XFELO

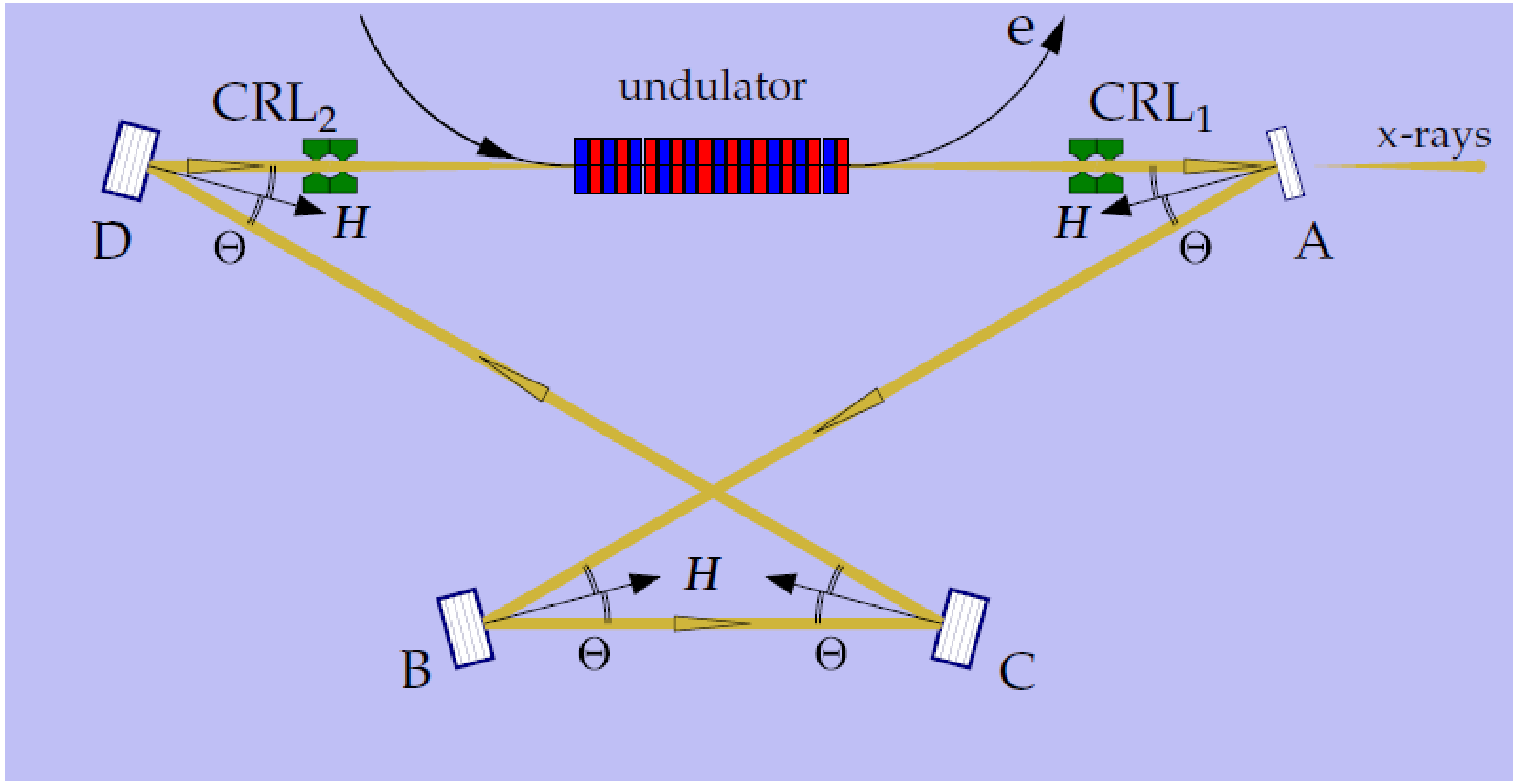

A, B, C, and D: Bragg crystals
CRL: Compound refractive lenses

H: Bragg crystal normal vector
θ: Diffraction angle

XFELO Spectra vs. N_{pass}

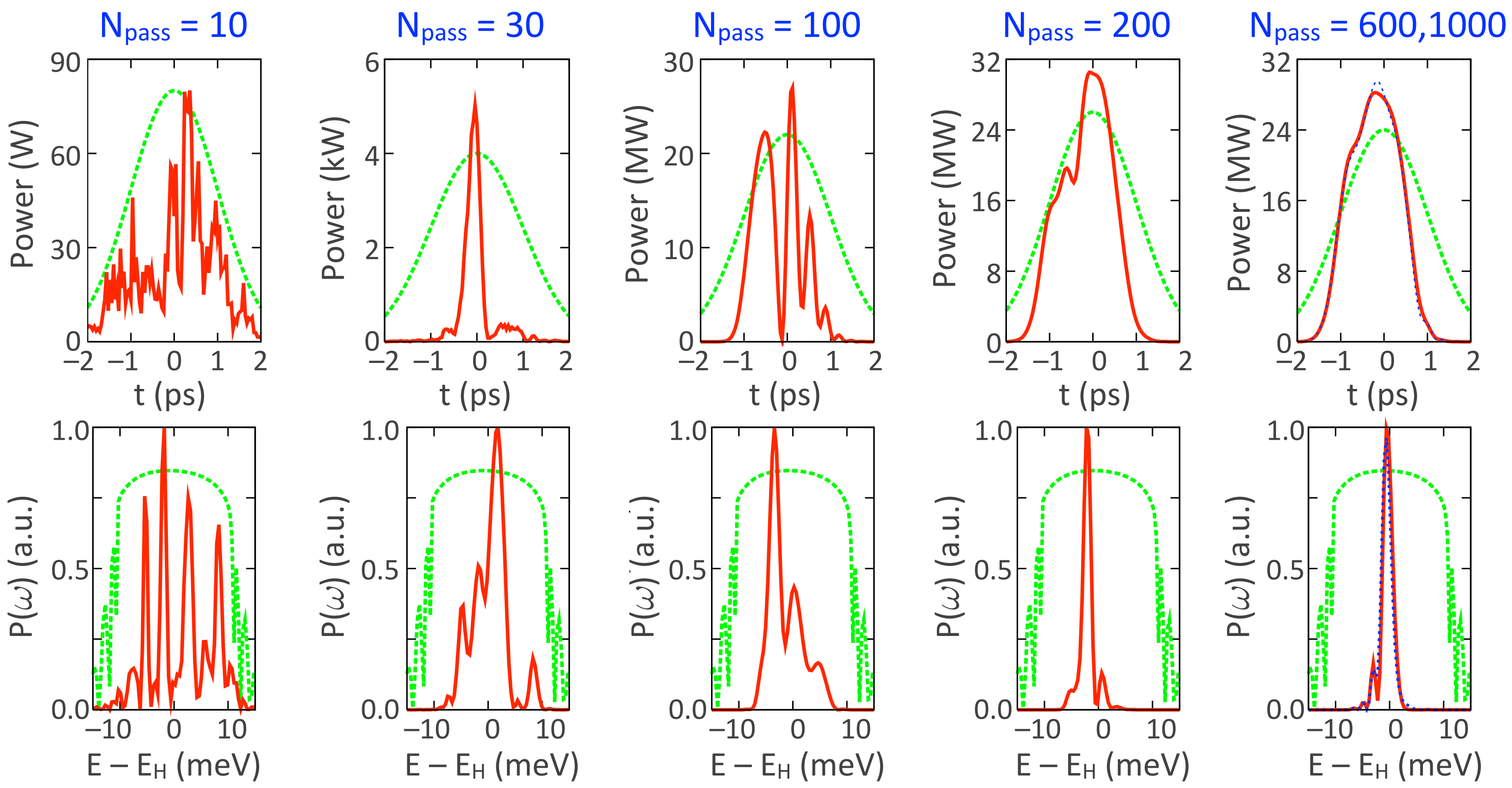

XFELO output spectra become narrower with N_{pass}

$$\left(\frac{\sigma_E}{E}\right) \sim \frac{1}{N_u} \frac{1}{\sqrt{N_{pass}}}$$

R.R. Lindberg et al., Phys. Rev. ST Accel. Beams, 14, 010701 (2011)

High-Gain Harmonic Generation (HGHG)

Harmonic Generation in an FEL

In the special case where the longitudinal distribution is periodic in phase

$$S(\psi) = \frac{a_0}{2} + Re\left\{\sum_{k=1}^{\infty} c_k \exp(ik\psi)\right\}$$

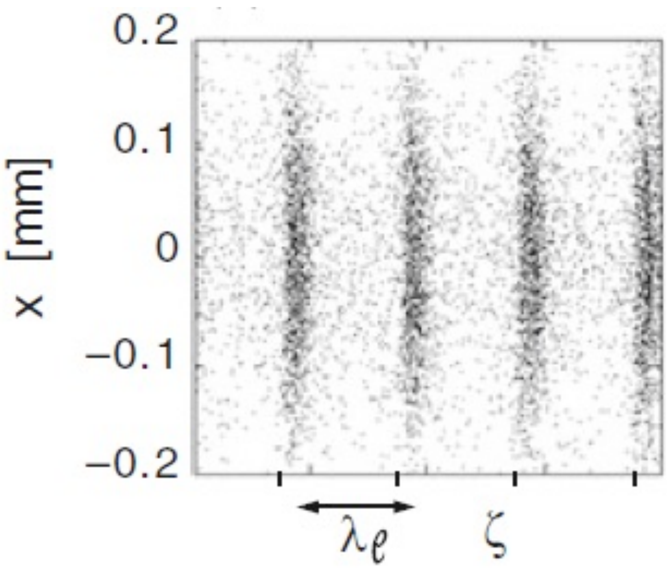

Complex Fourier coefficients

$$c_k = \frac{1}{\pi}\int_0^{2\pi} S(\psi)\exp(-ik\psi_n)d\psi$$

$$c_0 = a_0 = \frac{N}{\pi}$$

Strong bunching along the longitudinal coordinate ζ of the electron bunch translates into non-zero Fourier coefficients at multiple harmonic frequencies

1D FEL Simulation with Third Harmonic

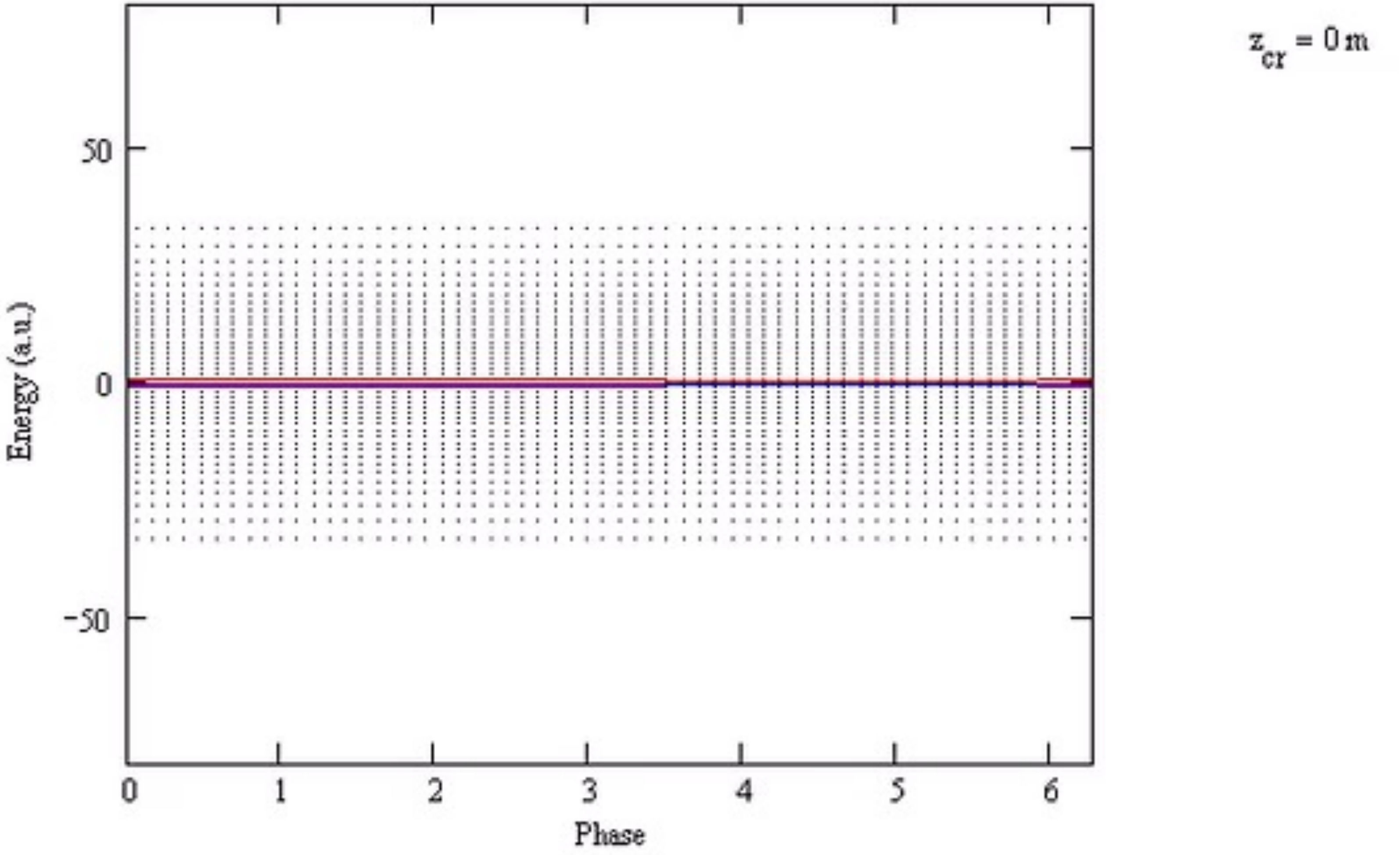

Principle of HGHG FEL

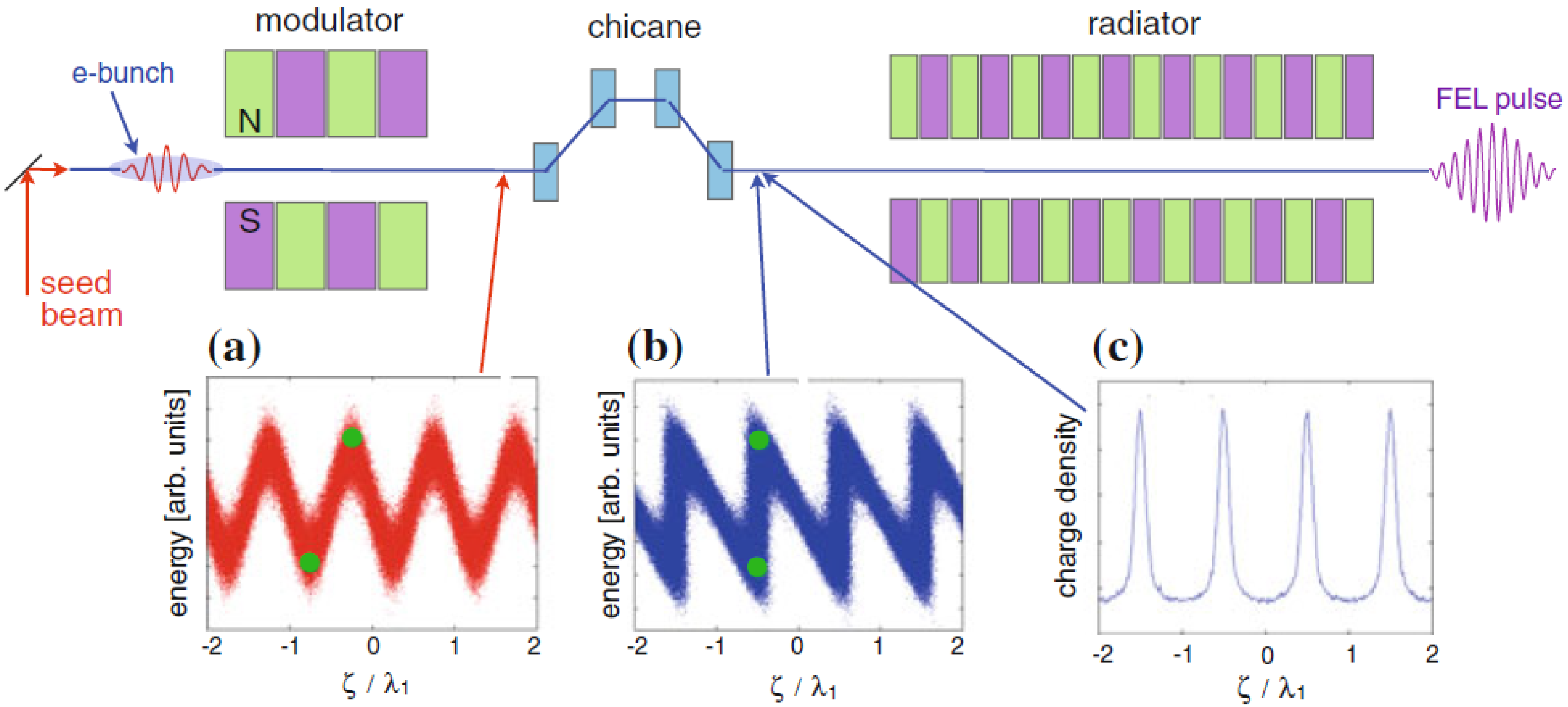

HGHG uses an external laser to modulate the electron energy in the **modulator**, followed by a **chicane** to converts the energy modulations into density modulations, and finally the bunched beam with high Fourier coefficients radiates coherently at a harmonic frequency in the **radiator**.

Dimensionless Variables

Dimensionless longitudinal position, ξ, which is defined as where s is the longitudinal position in meters, and λ is the wavelength of the laser used to modulate the beam.

$$\xi = \frac{2\pi s}{\lambda}$$

The energy of the electrons is described by the dimensionless energy deviation p which is given by:

$$p = \frac{\gamma - \gamma_0}{\sigma_\gamma}$$

Here σ_γ is the rms energy spread in the electron beam before the beam is modulated.

We will assume that the initial electron distribution is Gaussian in energy and is independent of the longitudinal coordinate. The initial dimensionless distribution is:

$$f_0(p) = \frac{N_0}{\sqrt{2\pi}} e^{-\frac{p^2}{2}}$$

Dimensionless Modulation Strength A

The prime denotes the phase space after modulation, while the unprimed coordinates are the phase space before modulation. The dimensionless parameter A represents the energy modulation strength as given by:

The energy modulation $\Delta\gamma$ depends on the laser power, laser transverse size, undulator length and undulator K

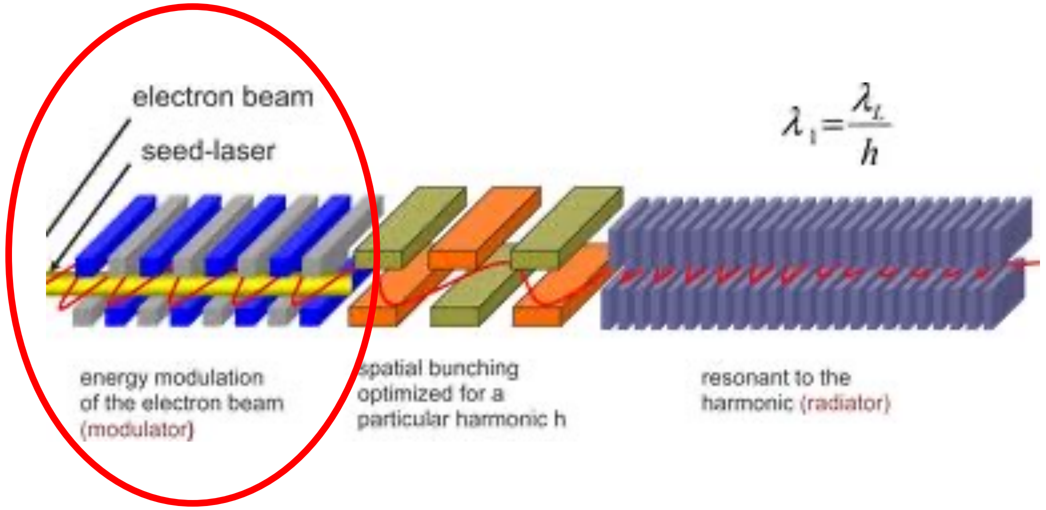

Electron phase space after the modulator

$$p' = p + A\sin(\xi)$$

$$A = \frac{\Delta\gamma}{\sigma_\gamma}$$

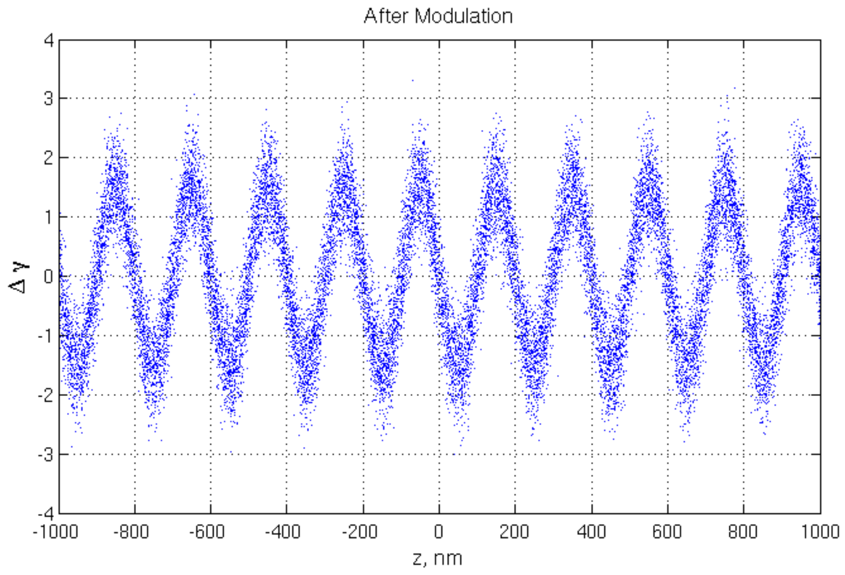

Dimensionless Buncher Strength *B*

Next the electron beam passes through a chicane where it undergoes bunching. The new phase space is:

$$\xi' = \xi + Bp'$$

$$\xi' = \xi + B(p + A\sin\xi)$$

The dimensionless parameter *B* describes the strength of the chicane, and is given by:

$$B = \frac{2\pi R_{56}\sigma_\gamma}{\lambda_1\gamma_0}$$

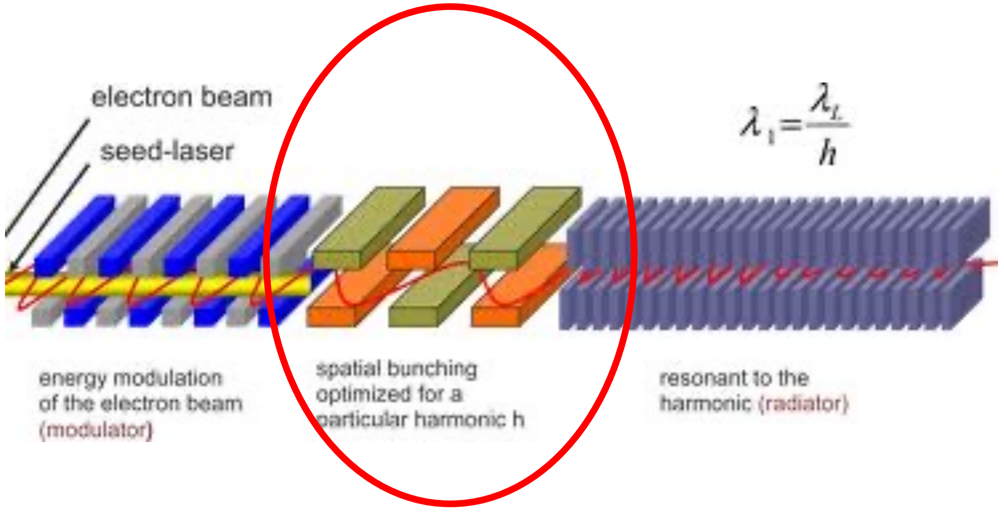

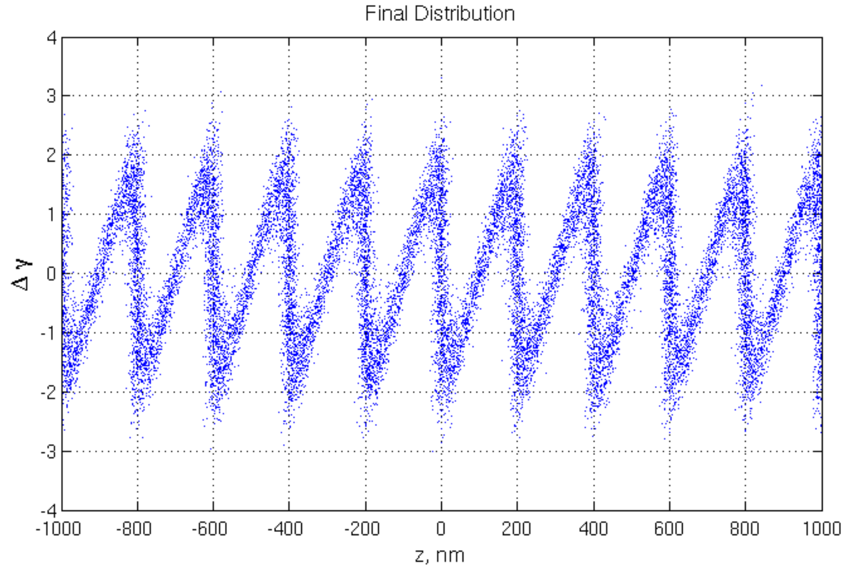

Phase-space Distribution

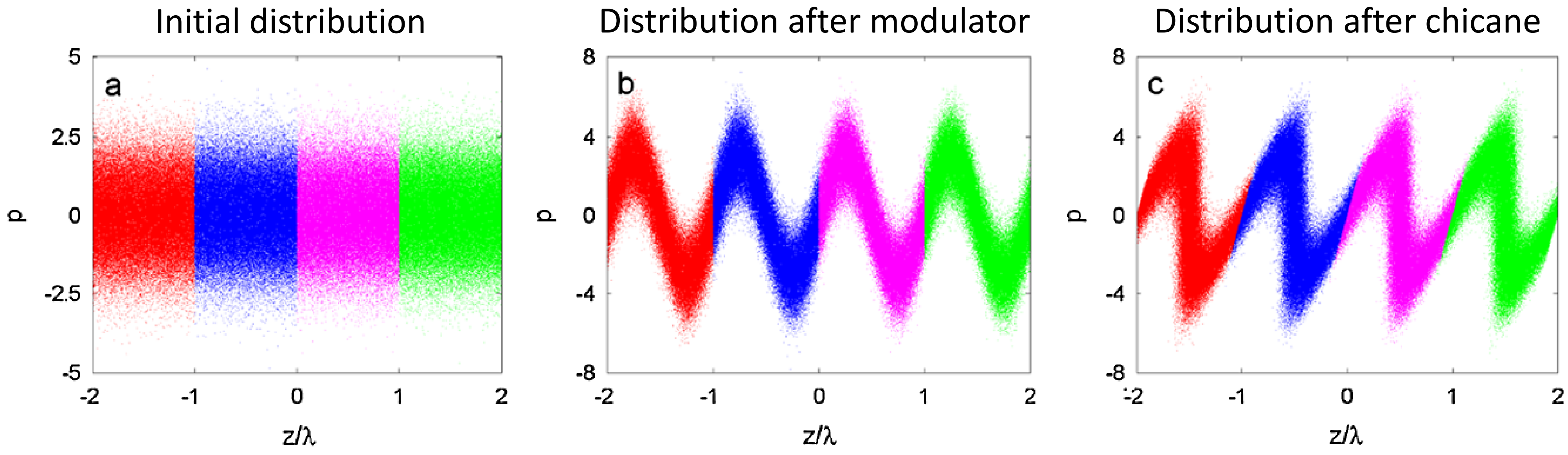

$$f_0(p) = \frac{N_0}{\sqrt{2\pi}} e^{-\frac{p^2}{2}}$$

$$f_1(\xi, p) = \frac{N_0}{\sqrt{2\pi}} e^{-\frac{(p - A\sin\xi)^2}{2}}$$

$$f_2(\xi, p) = \frac{N_0}{\sqrt{2\pi}} e^{-\frac{\left(p - A\sin(\xi - B_1 p)\right)^2}{2}}$$

Harmonic Bunching Factor

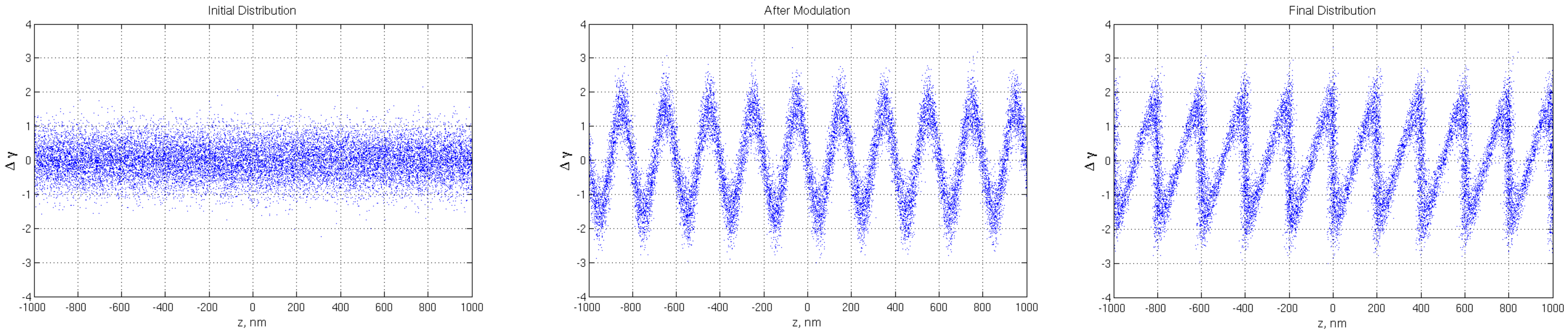

Initial electron line density

$$N_0 = \frac{I_p}{ec}$$

Bunching factor at the n^{th} harmonic

$$b(n) = \frac{1}{N_0} \left| \langle e^{-in\xi'} N(\xi') \rangle \right|$$

$$A = \frac{\Delta\gamma}{\sigma_\gamma}$$

Yu's formula for HGHG bunching

$$b(n) = J_n(nAB) \exp\left[-\frac{1}{2} n^2 B^2\right]$$

$$B = \frac{2\pi R_{56}\sigma_\gamma}{\lambda_1 \gamma_0}$$

Courtesy of Quinn Marksteiner (LANL)

Current Enhancement

Initial phase space

Initial current

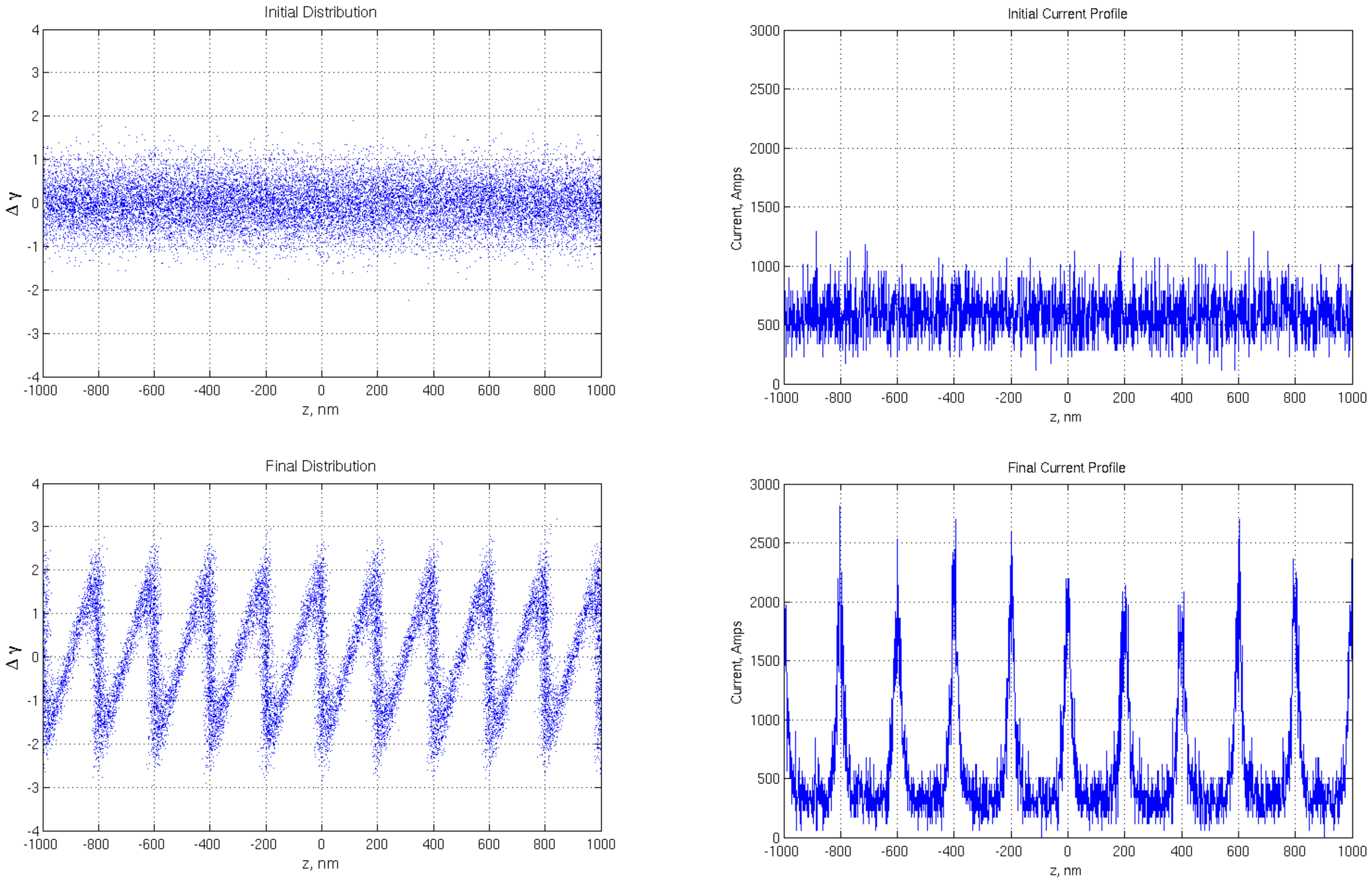

Final phase space

Final current

Courtesy of Quinn Marksteiner (LANL)

HGHG Demonstration in the UV and VUV

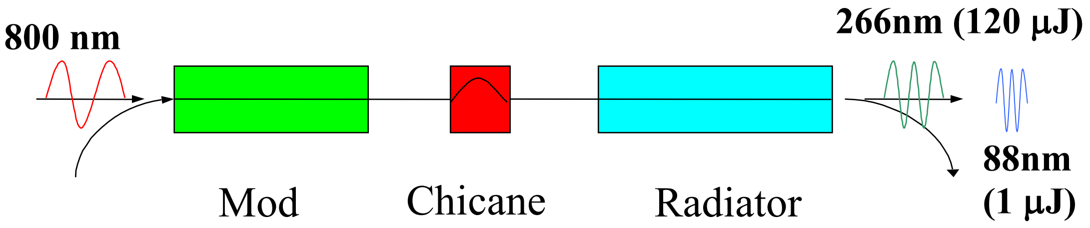

Spectra of HGHG (red) and unsaturated SASE (blue) under the same conditions. HGHG exhibits small shot-to-shot pulse energy fluctuations.

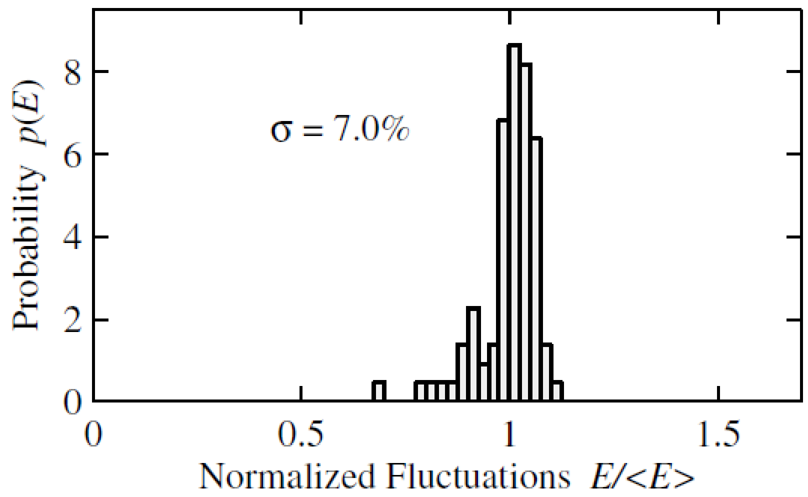

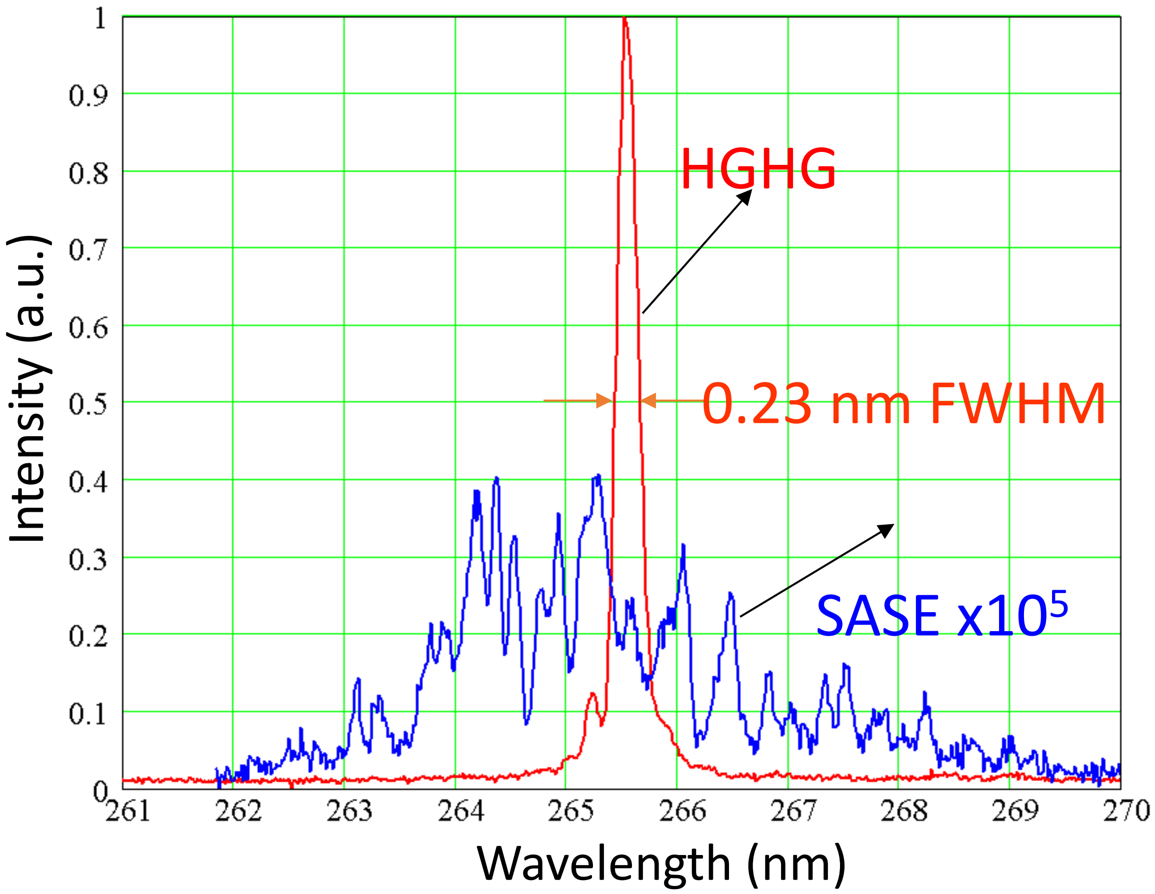

L. Yu et al., Phys. Rev. Lett. **91**, 074801-1 (2003).

Limitations of HGHG

Maximum harmonic bunching factor $$b(n) < \exp\left[-\frac{1}{2}n^2\left(\frac{\sigma_\gamma}{\Delta\gamma}\right)^2\right]$$

Small changes in phase of the laser translates to large phase changes in the harmonic

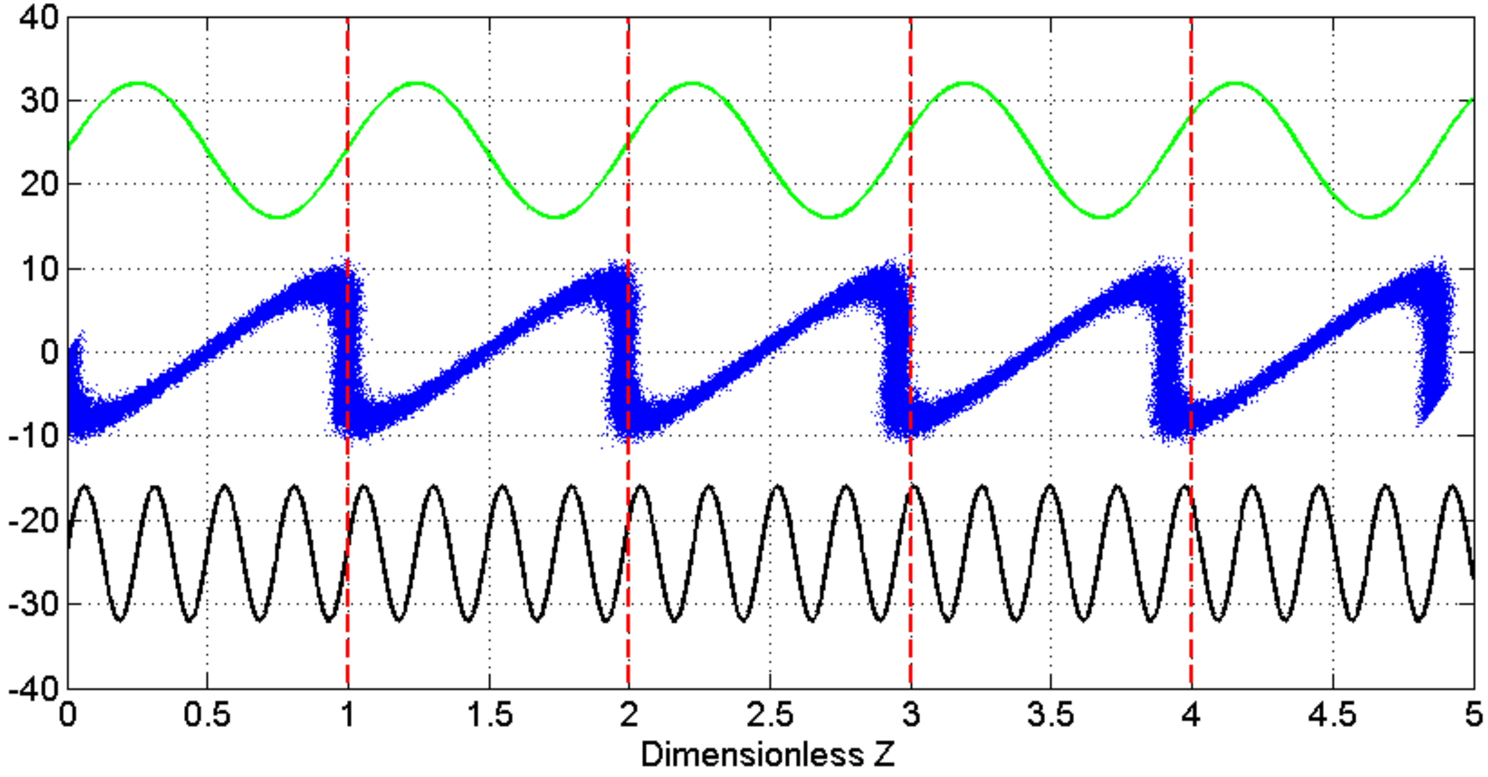

Echo Enabled Harmonic Generation

Shearing the Distribution with Large R_{56} (B)

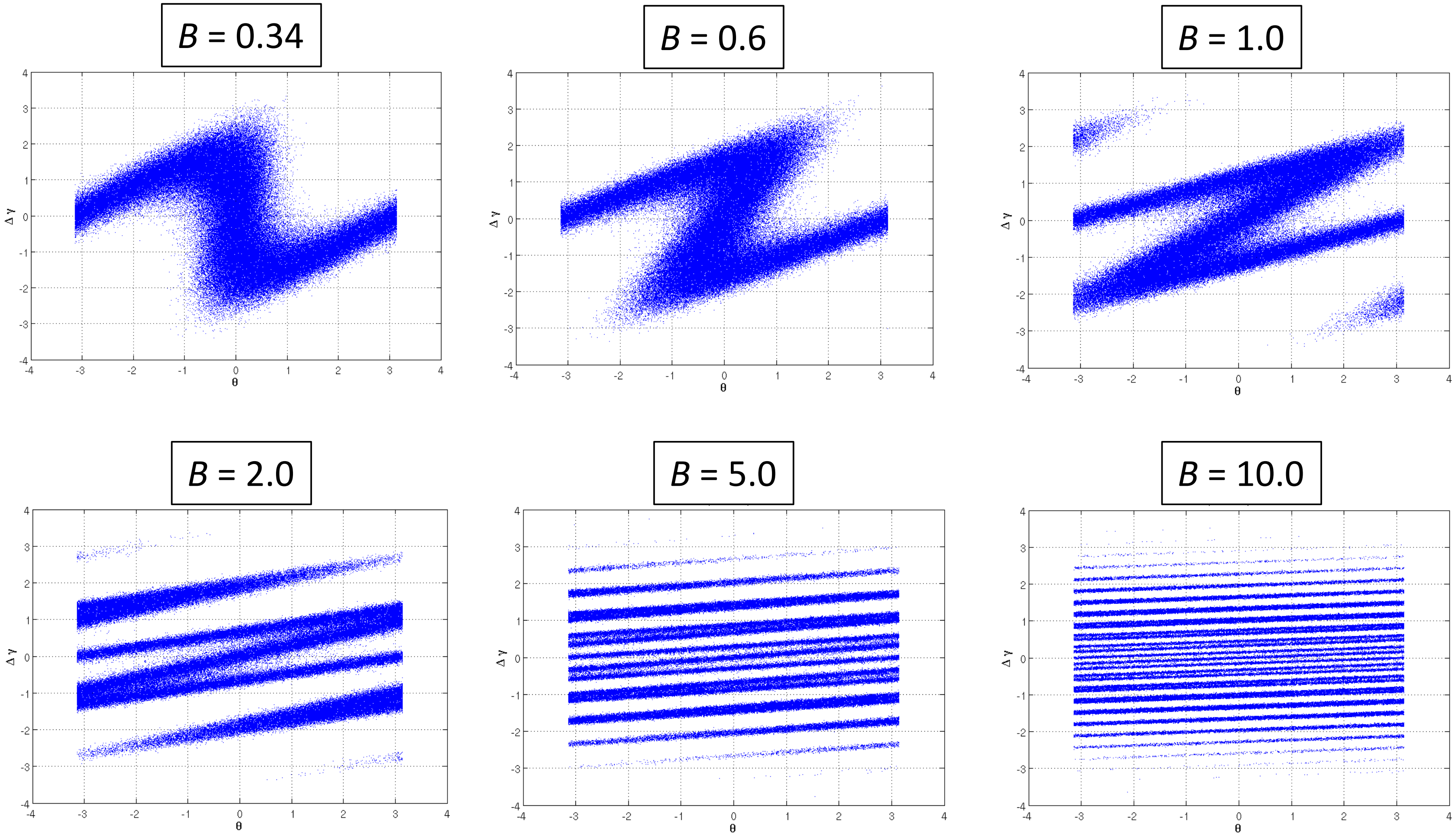

Principle of EEHG - 1

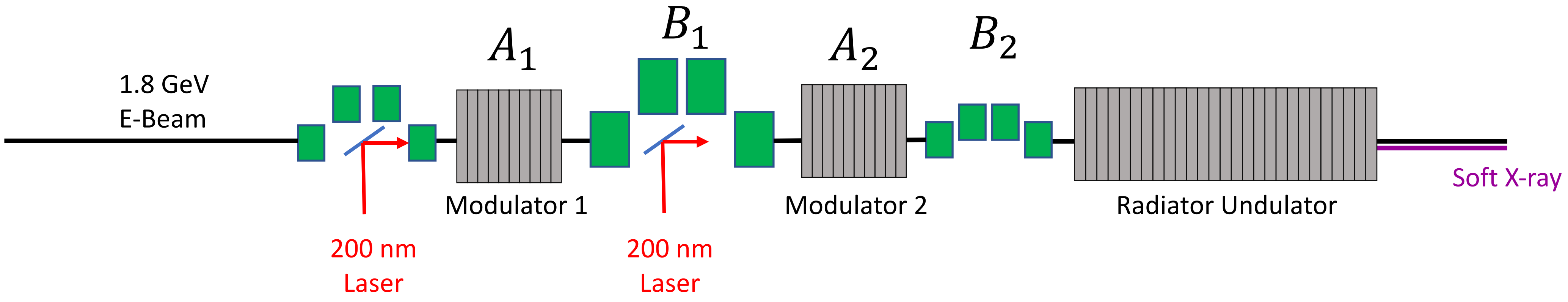

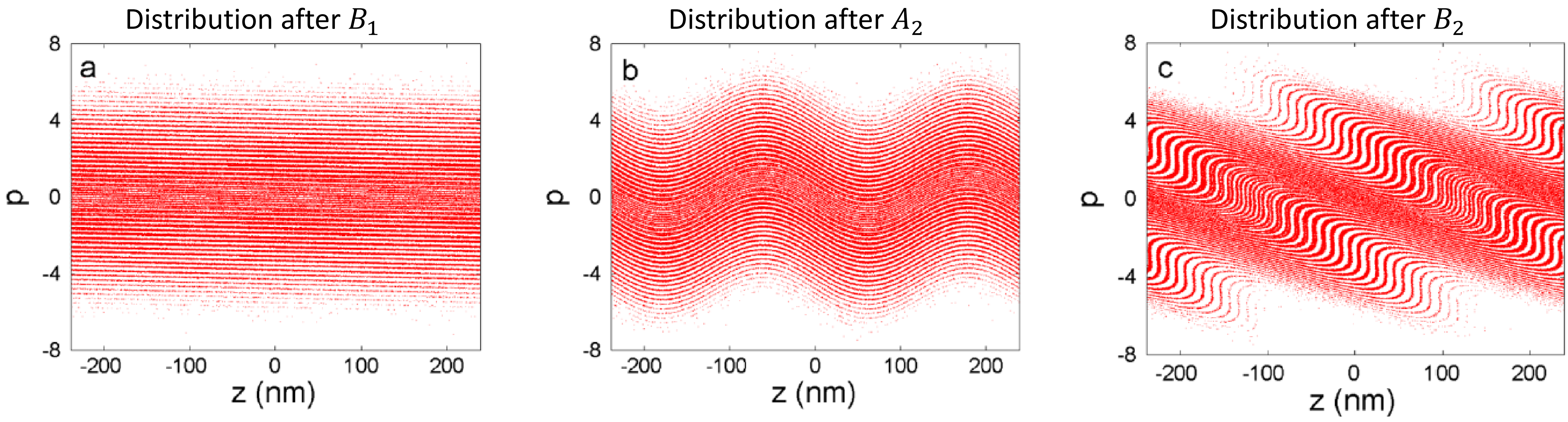

D. Xiang and G. Stupakov, Phys. Rev. ST Accel. Beams **12**, 030702 (2009).

Principle of EEHG - 2

Distribution after B_2

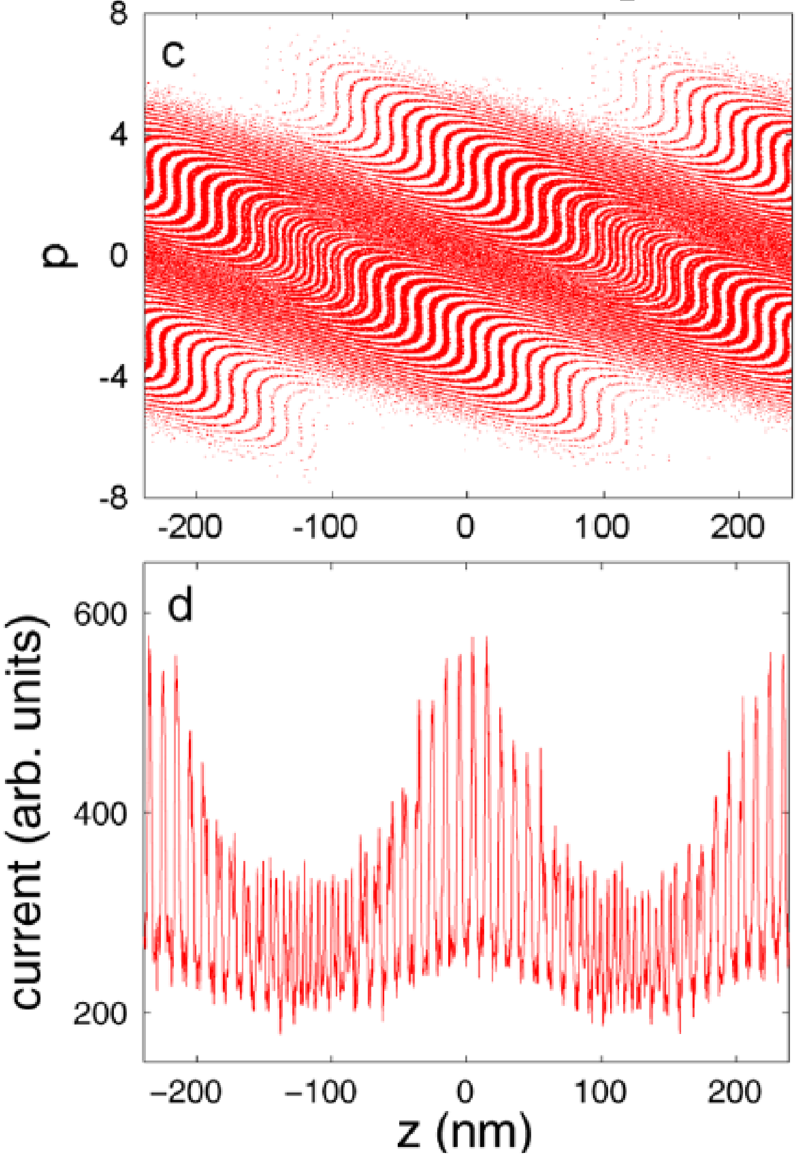

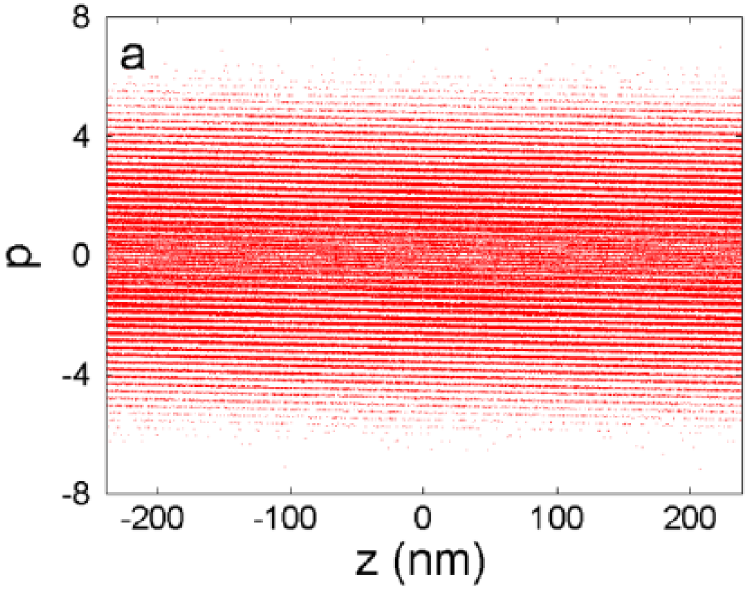

Distribution after B_1

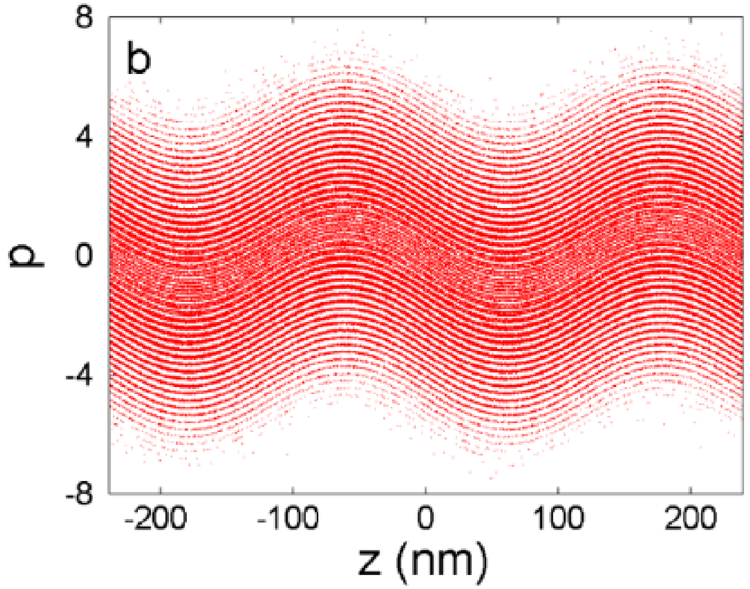

Distribution after A_2

D. Xiang and G. Stupakov, Phys. Rev. ST Accel. Beams **12**, 030702 (2009).

Phase Space after the First Modulator A_1

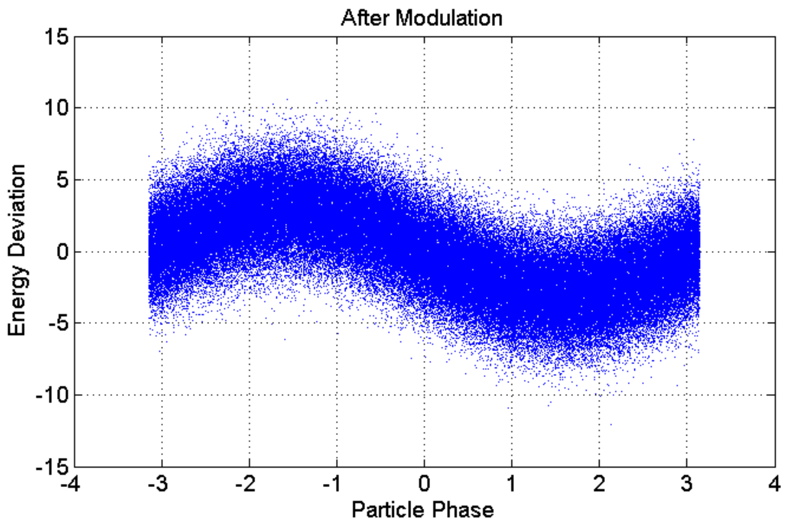

The first modulator imparts a sinusoidal modulation in energy, identical to the modulator in HGHG. Typical value of modulation is $A_1 \approx 3$.

The first modulator modifies phase space distribution according to:

$$p' = p + A_1 \sin(\xi)$$

Phase Space after the First Chicane B_1

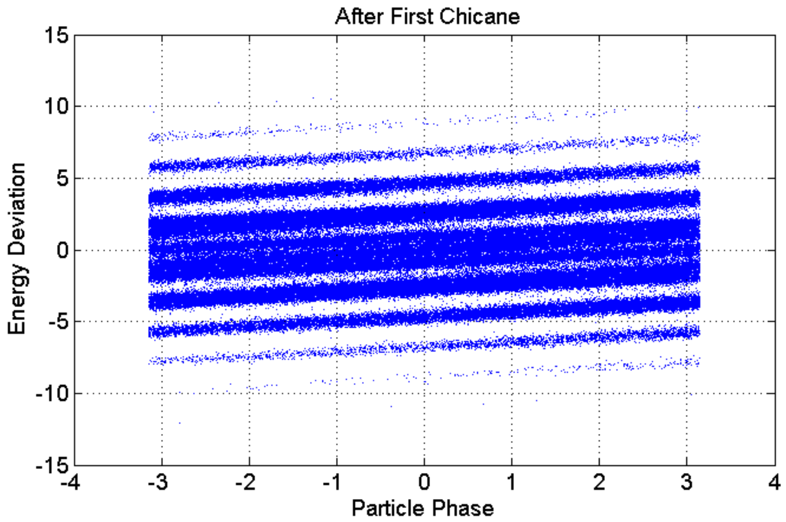

The first chicane following the first modulator produces energy stripes. The larger the chicane, the thinner each energy stripe will be. For the 24th harmonic, a value of bunching is $B_1 \approx 26.8$.

The first chicane modifies phase space distribution according to:

$$\xi' = \xi + B_1 p'$$

$$\xi' = \xi + B_1 (p + A_1 \sin \xi)$$

Phase Space after the Second Modulator A_2

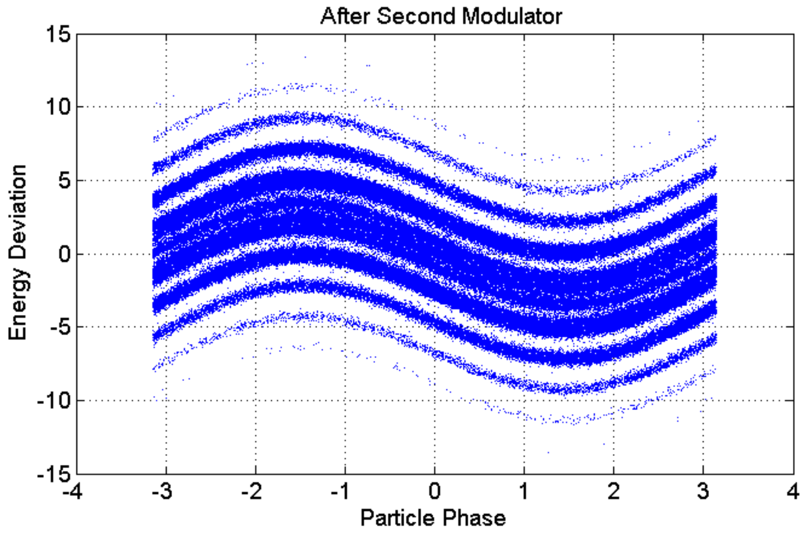

The second modulator gives each stripe a sinusoidal modulation.

$$\kappa = \frac{k_n}{k_1}$$

The second modulator modifies phase space distribution according to:

$$p'' = p' + A_2 \sin(\kappa\xi')$$

$$p'' = p + A_1 \sin\xi + A_2 \sin\{\kappa[\xi + B_1(p + A_1 \sin\xi)]\}$$

Phase Space after the Final Chicane B_2

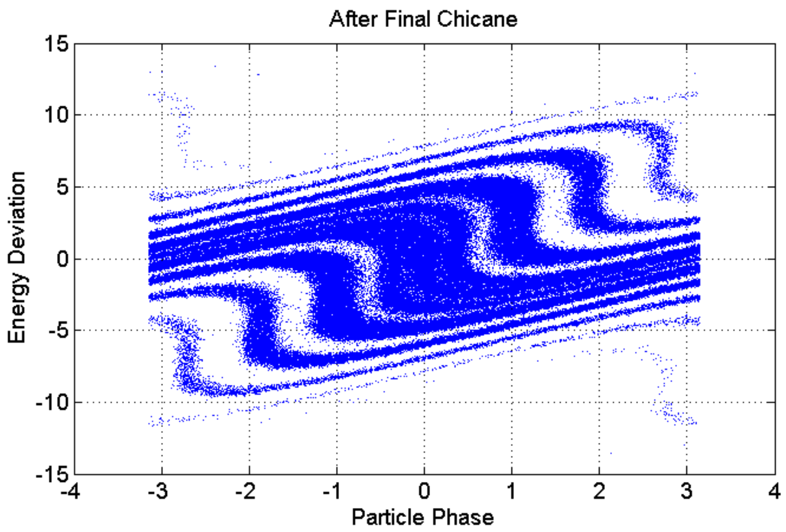

The final chicane rotates each of the stretched-out energy bands in phase space and produces microbunching at very high harmonics.

The final chicane modifies phase space distribution according to:

$$\xi'' = \xi + B_1(p + A_1 \sin \xi)$$

$$\xi'' = \xi + (B_1 + B_2)p + A_1(B_1 + B_2) \sin \xi + A_2 B_2 \sin(\kappa\xi + \kappa B_1 p + \kappa A_1 B_1 \sin \xi + \phi)$$

EEHG is better at high harmonics

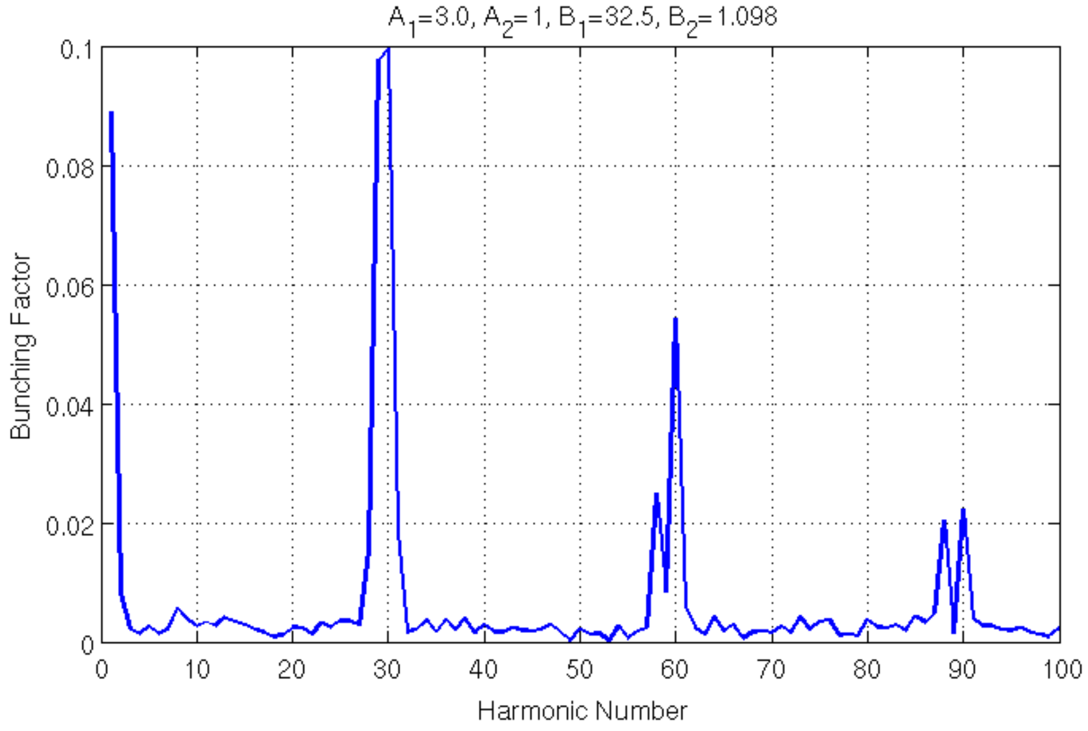

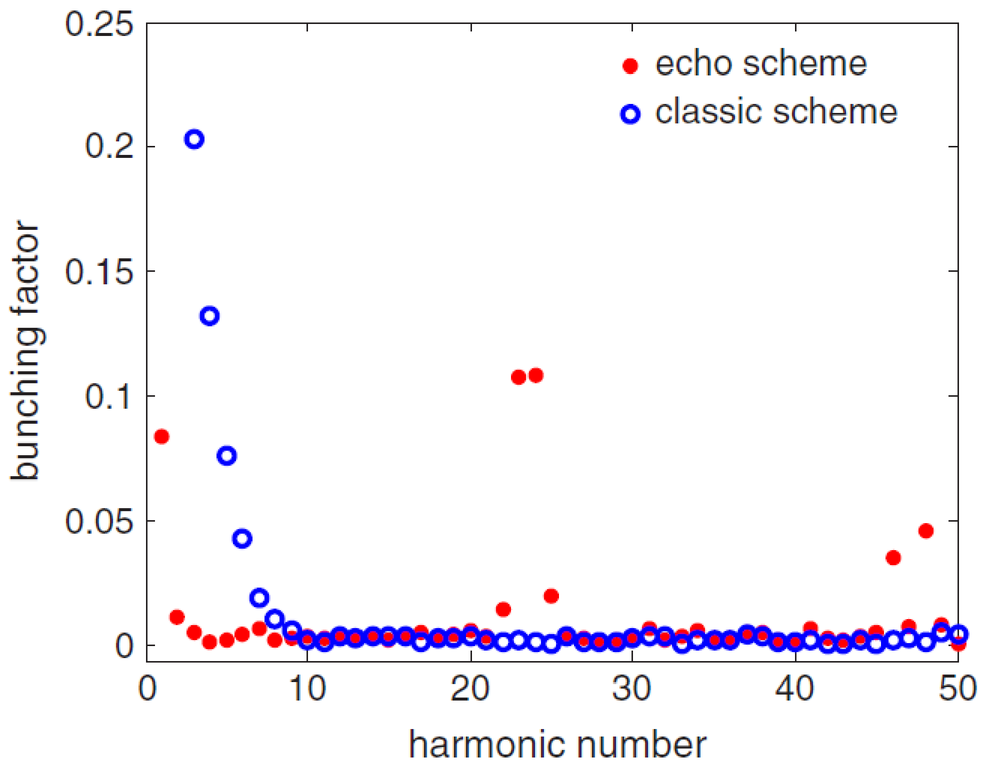

Scaling of EEHG bunching factor is favorable toward high harmonic generation.

$$b_n \approx \frac{0.39}{n^{1/3}}$$

Summary of Harmonic Generation

- FELs produce radiation at the fundamental and odd harmonics along the electron beam axis. The harmonic power decreases rapidly with harmonic number.

- High-Gain Harmonic Generation (HGHG) produces narrow-linewidth radiation at the harmonic of the injected laser. HGHG is sensitive to energy spread as well as phase and frequency changes in the laser.

- Echo-Enabled Harmonic Generation (EEHG) is an attractive technique to the generation of very high harmonic from the laser-driven harmonic FEL.